1 **Observation of new particle formation and measurement of sulfuric acid,**

2 **ammonia, amines and highly oxidized organic molecules at a rural site in**

3 **central Germany**

4

5

6 Andreas Kürten[1], Anton Bergen[1], Martin Heinritzi[1], Markus Leiminger[1], Verena Lorenz[1], Felix Piel[1],

7 Mario Simon[1], Robert Sitals[1], Andrea Wagner[1], and Joachim Curtius[1]

8

9 [1]Institute for Atmospheric and Environmental Sciences, Goethe University of Frankfurt, Frankfurt am

10 Main, Germany

11

12 Correspondence to: Andreas Kürten (kuerten@iau.uni-frankfurt.de)

13

14 **Abstract**

15

16 The exact mechanisms for new particle formation (NPF) under different boundary layer conditions are

17 not known yet. One important question is if amines and sulfuric acid lead to efficient NPF in the

18 atmosphere. Furthermore, it is not clear to what extent highly oxidized organic molecules (HOM) are

19 involved in NPF. We conducted field measurements at a rural site in central Germany in the proximity

20 of three larger dairy farms to investigate if there is a connection between NPF and the presence of amines

21 and/or ammonia due to the local emissions from the farms. Comprehensive measurements using a nitrate

22 Chemical Ionization-Atmospheric Pressure interface-Time Of Flight (CI-APi-TOF) mass spectrometer,

23 a Proton Transfer Reaction-Mass Spectrometer (PTR-MS), particle counters and Differential Mobility

24 Analyzers (DMAs) as well as measurements of trace gases and meteorological parameters were

25 performed. We demonstrate here that the nitrate CI-APi-TOF is suitable for sensitive measurements of

26 sulfuric acid, amines, a nitrosamine, ammonia, iodic acid and HOM. NPF was found to correlate with

27 sulfuric acid, while an anti-correlation with RH, amines and ammonia is observed. The anti-correlation

28 between NPF and amines could be due to the efficient uptake of these compounds by nucleating clusters

29 and small particles. Much higher HOM dimer (C19/C20 compounds) concentrations during the night

30 than during the day indicate that these HOM do not efficiently self-nucleate as no night-time NPF is

31 observed. Observed iodic acid probably originates from an iodine-containing reservoir substance but the

32 iodine signals are very likely too low to have a significant effect on NPF.

33

34

35 **1. Introduction**

36

The formation of new particles from gaseous compounds (nucleation) produces a large fraction of atmospheric aerosol particles (Zhang et al., 2012). While the newly formed particles have diameters between 1 and 2 nm they can grow and reach larger sizes, which enables them to act as cloud condensation nuclei (CCN, ~50 nm in diameter or larger). Removal processes such as coagulation scavenging due to larger pre-existing particles can be important if the growth rates (*GR*) for the newly formed particles are slow and/or if the coagulation sink (*CS*) is high. The climatic effect of nucleation depends strongly on the survival probability of the newly formed particles, i.e. if they reach CCN size, or not. Model calculations indicate that nucleation can account for ca. 50% of the CCN population globally (Merikanto et al., 2009). In addition to their climatic effect secondary particles can also influence the human health (Nel, 2005), or reduce visibility, e.g. in megacities (Chang et al., 2009).

New particle formation (NPF) is a global phenomenon and has been observed in many different environments (Kulmala et al., 2004). In most cases a positive correlation with the concentration of gaseous sulfuric acid has been observed (Sihto et al., 2006; Kuang et al., 2008). However, other trace gases, beside H_2SO_4 and H_2O, need to be involved in the formation of clusters, otherwise the high particle formation rates measured in the boundary layer cannot be explained (Weber et al., 1997; Kirkby et al., 2011). One ternary compound, which enhances the binary nucleation of sulfuric acid and water significantly, is ammonia. However, at the relatively warm temperatures of the boundary layer the presence of ammonia is probably not sufficient for reaching the observed NPF rates when acting together with sulfuric acid and water (Kirkby et al., 2011; Kürten et al., 2016). The same applies for ion-induced nucleation (IIN); the observed IIN rates for the binary and ternary system including ammonia are not high enough to explain the observations (Kirkby et al., 2011). Therefore, recent nucleation experiments focused on organic compounds acting as a ternary compound (beside H_2SO_4 and H_2O). Many studies indicate that amines have a very strong enhancing effect on nucleation (Kurtén et al., 2008; Chen et al., 2012; Glasoe et al., 2015). Indeed, a chamber experiment could show that the nucleation of sulfuric acid, water and dimethylamine (DMA) at 5°C and 38% RH produced particles at a rate, which is compatible with atmospheric observations in the boundary layer over a relatively wide range of sulfuric acid concentrations (Almeida et al., 2013). For sulfuric acid concentrations $<10^7$ molecule cm^{-3}, which are typical for the boundary layer, and dimethylamine mixing ratios of > ~10 pptv, nucleation was found to proceed at or close to the kinetic limit. This means every collision between sulfuric acid molecules, and clusters associated with DMA, leads to a larger cluster, which does not evaporate significantly (Kürten et al., 2014).

In principle, mass spectrometry using nitrate chemical ionization could be used to detect neutral clusters consisting of sulfuric acid and bases in the atmosphere. However, only few studies indicate that neutral nucleating atmospheric clusters consist of sulfuric acid and ammonia or amines (Zhao et al., 2011; Jiang et al., 2011), while other studies could not identify such clusters (Jokinen et al., 2012; Sarnela et al., 2015). A further outstanding issue is the question about the magnitude of the atmospheric amine mixing ratios at different locations. In the past several years the experimental tools for sensitive

online measurement of amines in the pptv-range became available (Hanson et al., 2011; Yu and Lee 2012). The reported amine levels reach from up to tens of pptv (Hanson et al., 2011; Freshour et al., 2014; You et al., 2014; Hellén et al., 2014) to < 0.1 pptv (Sipilä et al., 2015). It is therefore an important question if some of the reported mixing ratios could be biased high or low due to instrumental issues, or if the natural variability in the amine mixing ratios due to different source strengths can explain the differences.

Other possible contributors to particle formation are highly oxidized organic compounds (HOM) originating e.g. from the reaction of monoterpenes with atmospheric oxidants (Zhao et al., 2013; Ehn et al., 2014; Riccobono et al., 2014; Jokinen et al., 2015; Kirkby et al., 2016; Bianchi et al., 2016). From this perspective it seems likely that different nucleation pathways are possible and may dominate at different sites depending, e.g. on the concentration of sulfuric acid, amines, oxidized organic compounds and other parameters like temperature and relative humidity. Synergistic effects are also possible, e.g. it has been demonstrated that the combined effect of ammonia and amines can lead to more efficient particle formation with sulfuric acid and water than for a case where ammonia is not present (Glasoe et al., 2015). Due to the manifold possibilities for nucleation and the low concentrations of the growing clusters it is challenging to identify the dominating particle formation pathway from field measurements in an environment where many possible ingredients for nucleation are present at the same time. However, such measurements are necessary and previous measurements from Hyytiälä, Finland, underscored the importance of sulfuric acid, organic compounds and amines regarding NPF (Kulmala et al., 2013).

In this study, we have chosen to conduct measurements with an emphasis on the observation of NPF at a rural site in central Germany. The goal of this field campaign was to measure NPF in an amine rich environment in the vicinity of dairy farms, as cows are known to emit a variety of different amines as well as ammonia (Schade and Crutzen, 1995; Ge et al., 2011; Sintermann et al., 2014). The measurements were performed using different particle counters and particle size analyzers as well as trace gas monitors (O_3, SO_2 and NO_x). A Proton Transfer Reaction-Mass Spectrometer (PTR-MS) is used to determine the gas-phase concentration of monoterpenes and isoprene, whereas a chemical ionization time of flight mass spectrometer using nitrate primary ions (Jokinen et al., 2012; Kürten et al., 2014) is used for the measurement of sulfuric acid, amines, ammonia and highly oxidized organics.

2. Methods and Measurement Site Description

2.1 Measurement Site Description

The measurement site is located right next to a meteorological weather station operated by the German Weather Service (DWD measurement station Michelstadt-Vielbrunn/Odenwald, 49°43'04.4" N and

111 09°05'58.9" E, 452 m a.s.l.). The village Vielbrunn has a total of ~1300 inhabitants and is surrounded

112 by fields and forests. The next larger cities are Darmstadt (~35 km towards WNW) and Frankfurt/Main

113 (~50 km towards NNW). The site was chosen for several reasons: (i) three larger dairy farms are close

114 by, which should possibly enable us to study the effect of amines on new particle formation, (ii) it can

115 be regarded as typical for a rural or agricultural area in central Europe, (iii) the site is not too far away

116 from the University of Frankfurt, which allowed to visit the station for instrument maintenance on a

117 daily basis and (iv) since we could measure right next to a meteorological station infrastructure and

118 meteorological data from the DWD could be used.

119   In terms of studying the effect of amines on new particle formation we were expecting to see a direct

120 effect due to the local emissions from the dairy farms. Each of these farms is keeping a couple of hundred

121 cows in shelters, which are essentially consisting only of a roof and a fence such that the wind can easily

122 carry away the emissions. As mentioned in the introduction livestock are known to emit a variety of

123 amines as well as ammonia (Schade and Crutzen, 1995; Sintermann et al. 2014) both of which should

124 have an influence on new particle formation and growth (Almeida et al., 2013; Lehtipalo et al., 2016).

125 The farms are located in the West (~ 450 m distance), South-South-West (~ 1100 m distance) and South-

126 East (~ 750 m distance) of the station, respectively.

127   One further aspect that should be considered is the fact that the site is also surrounded by forests

128 (mixed type of coniferous and deciduous trees, at least 1 km away). Consequently, emissions of, e.g.

129 monoterpenes ($C_{10}H_{16}$ compounds), can also potentially influence new particle formation as recent

130 studies indicate that their oxidation products can contribute to NPF and particle growth (Schobesberger

131 et al., 2013; Riccobono et al., 2014; Ehn et al., 2014; Kirkby et al., 2016).

132

133 **2.2 CI-APi-TOF**

134

135 The key instrument for the data discussed in this study is the Chemical Ionization-Atmospheric Pressure

136 interface-Time Of Flight mass spectrometer (CI-APi-TOF). The instrument was first introduced by

137 Jokinen et al. (2012) and the one used in the present study is described by Kürten et al. (2014). The CI-

138 APi-TOF draws a sample flow of 8.5 slm (standard liters per minute), which interacts with nitrate

139 primary ions (($HNO_3)_{0-2}NO_3^-$) within an ion reaction zone at ambient pressure (~ 50 ms reaction time).

140 The primary ions are generated from the interaction of HNO_3 in a sheath gas and a negative corona

141 discharge (Kürten et al., 2011). The ion source is based on the design by Eisele and Tanner (1993) for

142 the measurement of sulfuric acid. The primary and product ions are drawn into the first stage of a vacuum

143 chamber through a pinhole (~350 µm diameter). Quadrupoles in the first and a second stage of the

144 chamber, operated in rf-only mode, are used to guide the ions. A lens stack in a third stage focuses and

145 prepares the ions energetically before they enter the time of flight mass spectrometer (Aerodyne

146 Research Inc., USA and Tofwerk AG, Switzerland). This mass spectrometer has a mass resolving power

147 of ~4000 Th/Th and a mass accuracy of better than 10 ppm. These characteristics allow the elemental

148   identification of unknown ions, i.e. different species having the same nominal (integer) m/z ratio can be

149   separated due to their mass defect. Using isotopic patterns for an expected ion composition supports the

150   ion identification. For the data analysis the software tofTools (Junninen et al., 2010) is used within the

151   Matlab environment.

152   Previous work has shown that the CI-APi-TOF can be used for highly sensitive measurements of

153   sulfuric acid (Jokinen et al., 2012), clusters of sulfuric acid and dimethylamine (Kürten et al., 2014),

154   organic compounds with very low volatility (Ehn et al., 2014) and dimethylamine (Simon et al., 2016).

155   Sulfuric acid and its clusters can be detected after donating a proton to the primary ions, i.e.,

156    $(H_2SO_4)_n + (HNO_3)_{m=0-2}NO_3^- \rightarrow (H_2SO_4)_{n-1}(HNO_3)_{k=0-2}HSO_4^- + (m-k+1)(HNO_3)$ (R1)
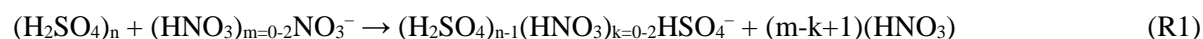
157   whereas the low volatility organic compounds (HOM) are detected after clustering with NO_3^-, i.e.,

158    $HOM + (HNO_3)_{m=0-2}NO_3^- \rightarrow (HOM)(HNO_3)_{k=0-2}NO_3^- + (m-k)(HNO_3)$.   (R2)

159   In both reactions (R1) and (R2) the presence of water has been neglected for simplicity. The

160   measurement of amines is possible because they can be associated with nitrate cluster ions (Section 3.6).

161   Generally, the quantification of a substance is derived with the following equation:

162

163    $$concentration = C \cdot ln\left(1 + \frac{\sum product\ ion\ count\ rates}{\sum primary\ ion\ count\ rates}\right).$$ (1)

164

165   Equation (1) relates the sum of the product ion count rates to the sum of the primary ion count rates.

166   Using a calibration constant C the concentration of a neutral substance can be determined. In the case

167   of the sulfuric acid concentration ($[H_2SO_4]$) the product ion count rates are due to HSO_4^- and

168    $(HNO_3)HSO_4^-$, while the primary ion count rates include NO_3^-, $(HNO_3)NO_3^-$ and $(HNO_3)_2NO_3^-$. The

169   calibration constant has been determined as 6×10^9 molecule cm^{-3} (Kürten et al., 2012).

170   The same calibration constant has also been used for the quantification of HOM. However, in this

171   case the mass dependent transmission of the CI-APi-TOF was taken into account by the method of

172   Heinritzi et al. (2016). This requires an additional correction factor in equation (1) which is around 0.4

173   for the m/z range 300 to 400 Th and 0.22 for the range 500 to 650 Th; these factors take into account

174   only the transmission as function of the m/z value, while assuming the same ionization efficiency as for

175   sulfuric acid, which has been shown to be a valid assumption by Ehn et al. (2014). The quantification

176   of amines will be detailed in Section 3.6. Table 1 gives an overview of the identified ion signals used in

177   the further analysis evaluating sulfuric acid monomer and dimer concentrations as well as amine,

178   nitrosamine, ammonia and iodic acid signals (further explanations will be given in the following

179   sections).

180   Regarding the loss of sample molecules within the inlet line of the CI-APi-TOF we expect only a

181   minor effect. As the sample line has a total length around 1 m, a very high flow rate was applied over

182   most of the inlet length (Berresheim et al., 2000). Only for the last ~15 cm the flow of 8.5 slm was

183   applied taking the sample from the center part of the first inlet stage where the inlet has a significantly

184   larger diameter (5 cm instead of 1 cm for the last part) to avoid wall contact of the relevant portion of

185   the sampled air.

186

187   **2.3 PTR-MS**

188

189   Volatile Organic Compounds (VOCs) were measured with a calibrated Proton Transfer Reaction-Mass

190   Spectrometer (PTR-MS using a quadrupole mass spectrometer, IONICON GmbH, Innsbruck, Austria).

191   The instrument inlet was heated to 60°C and the same temperature was applied to the ion drift tube. The

192   drift tube was operated at an E/N of 126 Td in order to minimize the formation of protonated water

193   clusters while maintaining a high sensitivity (E/N is the ratio between the electric field strength E in V

194   cm^{-1} and the number density N of gas molecules in cm^{-3}, see Blake et al., 2009).

195   A calibration of the instrument was performed prior to the campaign with a gas mixture containing

196   several VOCs at a known volume mixing ratio (Ionimed-VOC-Standard, Innsbruck, Austria), including

197   isoprene, α-pinene, and acetone amongst others. The calibration was performed for a relative humidity

198   range of 0 to 100 % (steps of 20 %) at room temperature. However, especially for α-pinene (measured

199   at 81 and 137 Th), the sensitivity of the PTR-MS operating at the rather high E/N was not depending on

200   relative humidity. For isoprene (measured at 41 and 69 Th), a higher RH led to lower fragmentation

201   inside the instrument, but this did not affect the overall sensitivity much (<5 % decrease from 20 to

202   100%).

203   The PTR-MS cannot readily distinguish between different monoterpenes as all have the same

204   molecular weight, so only the sum of monoterpenes could be measured. However, since α-pinene is

205   often the most abundant monoterpene in continental mid latitudes (Geron et al., 2000; Janson and de

206   Serves, 2001) and the reaction rate constants for different monoterpenes are rather similar (Tani et al.,

207   2003; Cappellin et al., 2012) our estimation of total monoterpene concentration should not be affected

208   by large errors.

209

210   **2.4 Other instrumentation**

211

212   Trace gas monitors were used to measure the mixing ratios of sulfur dioxide (Model 43i TLE Trace

213   Level SO_2 Analyzer, Thermo Scientific), ozone (Model 400, Ozone Monitor, Teledyne API) and

214   nitrogen oxides (NO_x, Ambient NO_x-Monitor APNA-360, Horiba). These instruments were calibrated

215   once before the campaign with known amounts of trace gases and dry zero air was applied on a daily

216   basis for a duration of at least half an hour in order to take instrument drifts into account. The detection

217   limits of the gas monitors are 0.05 ppbv for the SO_2 monitor (for a 5 minute integration time),

218   approximately 0.5 ppbv for the NO_x monitor and 0.5 to 1 ppbv for the O_3 monitor.

219   Further instruments used include condensation particle counters (CPCs) and differential mobility

220   analyzers (DMAs). The CPCs 3025A and 3010 (TSI, Inc.) were used to determine the total particle

concentration above their cut-off sizes of 2.5 and 10 nm, respectively. A Scanning Mobility Particle Sizer (SMPS) from TSI (Model 3081 long DMA with a CPC 3776) determined the particle size distribution between 16 and 600 nm. The smaller size range was covered by a nDMA (Grimm Aerosol Technik, Germany) and a TSI CPC 3776 for diameters between 3 and 40 nm. The combined size distribution can be used to calculate the condensation/coagulation sink towards certain trace gases (e.g. sulfuric acid) or particle diameters.

Meteorological parameters were both obtained from our own measurements with a Vaisala sonde (Model WXT 520), which yielded the temperature, RH, wind speed and direction as well as the amount of precipitation. The same parameters are also available for the Vielbrunn meteorological station from the DWD; additionally, values for the global radiation were provided from the DWD.

3. Results

3.1 Meteorological conditions and overview

The intensive phase of the campaign was from May 18 to June 7, 2014 (21 campaign days). Figure 1 shows an overview of the meteorological conditions, i.e. temperature, relative humidity, global radiation and precipitation. The size distribution of small particles (Fig. 1, bottom panel) was measured by the nDMA. In addition, the condensation sink calculated for the loss of sulfuric acid on aerosol particles is also shown taking into account the full size distribution (up to 600 nm).

The first part of the campaign (including May 22) was characterized by warm temperatures and sunny weather without precipitation. Between May 22/23 and May 31 the weather conditions were less stable with colder temperatures and some precipitation events. Especially on May 29 a strong drop in temperature and the condensation sink was observed, due to a cold front followed by the passage of relatively clean air. From May 31 on temperatures were increasing again and it was mostly sunny with only two rain events on June 3 and June 4.

Elevated concentrations of small particles could be observed on almost every day. However, new particle formation from the smallest sizes (around 3 nm) followed by clear growth were seen only on 6 days out of 21 (i.e. 29%). These events, which were also used for the calculation of new particle formation rates (Section 3.9), are highlighted in the bottom panel of Fig. 1 by the dark gray arrows. The presence of small particles was also observed on several other days, however, the events were either relatively weak, or no clear particle growth was observable.

3.2 Trace gas measurements

257 The trace gas measurements are shown in Fig. 2. Typical maximum day-time ozone mixing ratios ranged
258 from ~40 to 75 ppbv (Fig. 2, upper panel). The sulfur dioxide levels were between 0.05 and a maximum
259 of 2 ppbv with average values around 0.3 ppbv (Fig. 2, upper panel). Especially during the passage of
260 clean air on May 29 and May 30 the SO_2 levels were quite low. NO_2 mixing ratios showed a distinct
261 diurnal pattern with a minimum in the late afternoon and an average mixing ratio around 3 ppbv (Fig.
262 2, middle panel, see also Fig. 8). The NO mixing ratios were about a factor of 5 lower compared to NO_2
263 on average (Fig. 2, middle panel, see also Fig. 8); similar values were reported for another rural site in
264 Germany (Mutzel et al., 2015). The maximum sulfuric acid concentrations were reached around noon
265 and ranged between ~1×10^6 and 2×10^7 molecule cm^{-3} (Fig. 2, lower panel, see also Fig. 3), which is
266 comparable to other sites (Fiedler et al., 2005; Petäjä et al., 2009). The total monoterpene and isoprene
267 mixing ratios measured by the PTR-MS were similar to each other with values between ~0.03 and 1
268 ppbv (Fig. 2, lower panel). Mixing ratios in the same range have also been reported for the boreal forest
269 (Rantala et al., 2014).

270

271 3.3 H_2SO_4 measurement and calculation from proxies

272

273 Figure 3 shows the average diurnal sulfuric acid concentration along with other data, which will be
274 discussed in later sections. The maximum average $[H_2SO_4]$ around noon was ~3×10^6 molecule cm^{-3}; the
275 error bars represent one standard deviation.
276   Recently, Mikkonen et al. (2011) introduced approximations to calculate sulfuric acid as a function
277 of different proxies. Since the relevant parameters (sulfur dioxide mixing ratio, global radiation, relative
278 humidity and condensation sink) are available, we have used the following formula to approximate the
279 sulfuric acid concentration (Mikkonen et al., 2011):

280

$$281 \qquad [H_2SO_4]_{proxy} = a \cdot k(T,p) \cdot [SO_2]^b \cdot Rad^c \cdot RH^d \cdot CS^e. \qquad\qquad (2)$$

282

283 The $[H_2SO_4]$ (expressed in molecule cm^{-3}) is calculated as a function of the SO_2 mixing ratio (in ppbv),
284 the global radiation Rad (in W m^{-2}), the relative humidity RH (in %), the condensation sink CS (in s^{-1}),
285 a rate constant k, which depends on ambient pressure p and temperature T (see definition for k by
286 Mikkonen et al., 2011) and a scaling factor a. A least square fit made with the software IGOR yields the
287 coefficients $a = 1.321\times10^{15}$, $b = 0.913$, $c = 0.990$, $d = -0.217$ and $e = -0.526$ (linear correlation coefficient,
288 Pearson's r, is 0.87). Following the recommendations given by Mikkonen et al. (2011) we restricted the
289 data used in the derivation of the parameters to conditions where the global radiation was equal or larger
290 than 50 W m^{-2}. In addition, a simpler formulation was also tested, which neglects the dependence on RH
291 and CS:

292

$$293 \qquad [H_2SO_4]_{proxy'} = a' \cdot k(T,p) \cdot [SO_2]^{b'} \cdot Rad^{c'}. \qquad\qquad (3)$$

294

295 Here, the coefficients $a' = 1.343 \times 10^{16}$, $b' = 0.786$ and $c' = 0.941$ yield good agreement (linear correlation

296 coefficient, Pearson's r, is 0.85) between calculated and measured $[H_2SO_4]$. Figure 4 shows a

297 comparison between the two approximation methods and the measured sulfuric acid for the full

298 campaign (when $Rad \geq 50$ W m^{-2}). In almost all cases the predicted 5 minute averages are within a factor

299 of 3 of the measured values for both methods. This indicates that even the simpler method (equation (3))

300 can yield relatively accurate results for the conditions of this study. This is probably due to the fact that

301 RH and CS show only relatively small variations over the duration of the campaign and it would

302 therefore not be absolutely necessary to include these factors in the sulfuric acid calculation.

303 Nevertheless, whenever the data are available we recommend to use the more detailed parameterization

304 (equation (2)) as it treats the sulfuric acid concentration calculation more rigorously. The parameters

305 found are in good agreement with the ones reported by Mikkonen et al. (2011) for different sites.

306

307 **3.4 Calculated OH**

308

309 For further data evaluation knowledge of the OH concentrations is useful. In this study the hydroxyl

310 radical concentration is required to derive an estimated concentration of the iodine species OIO (Section

311 3.5) and for a comparison of conditions during nucleation and no nucleation days (Section 4). Since

312 there was no direct measurement of the hydroxyl radical available, only an estimation based on other

313 measured parameters can be made. This estimation is based on the assumption that most of the sulfuric

314 acid is produced from the reaction between SO_2 and OH. Using the condensation sink CS the balance

315 equation between production and loss at steady-state can be used to derive the OH:

316

317 $$[OH] \quad = \frac{CS \cdot [H_2SO_4] - k_{X+SO_2} \cdot [X] \cdot [SO_2]}{k_{OH+SO_2} \cdot [SO_2]} \approx \frac{CS \cdot [H_2SO_4]}{k_{OH+SO_2} \cdot [SO_2]}.$$ (4)

318

319 Recently it was discovered that there are also other species capable of oxidizing SO_2 to SO_3 (which lead

320 to subsequent production of H_2SO_4 due to further reactions with O_2 and H_2O) (Mauldin et al., 2012).

321 Those species X, e.g. stabilized Criegee Intermediates (sCI) can be formed via the ozonolysis of alkenes

322 (e.g. isoprene, α-pinene, limonene) (Mauldin et al., 2012; Berndt et al., 2014). Therefore, if some H_2SO_4

323 is generated from sCI reactions with SO_2, then the calculated OH is an upper estimate. During the day

324 this effect should be relatively small, i.e. < 50% (Boy et al., 2013; Sarwar et al., 2013), although Berndt

325 et al. (2014) state that no final answer can be given regarding the effect of the sCI on the sulfuric acid

326 formation because it depends strongly on the sCI structure and competitive reactions between sCI and

327 water vapor. However, it should also be noted that the reaction between alkenes and ozone generates

328 not only sCI but also OH at significant yields (e.g. the OH yield for the reaction of α-pinene and O_3 is

329 ca. 0.77, Forester and Wells, 2011) and that the OH produced via this mechanism is taken into account

330   by equation (4). Data from Sipilä et al. (2014) further suggest that the production of sulfuric acid from

331   sCI oxidation of SO_2 is probably minor compared to that from OH and SO_2. For these reasons we have

332   decided to calculate the [OH] not only for the day time but for the full day. The derived diurnal pattern

333   of [OH] is shown in Fig. 3 with a maximum concentration of 1×10^6 molecule cm^{-3} around noon, which

334   is in good agreement with other studies where OH was measured directly (Berresheim et al., 2000;

335   Rohrer and Berresheim, 2006; Petäjä et al., 2009).

336

337   **3.5 Iodic acid (HIO_3) and OIO**

338

339   The high resolution CI-APi-TOF mass spectra revealed the presence of iodine containing substances. It

340   can be ruled out that these signals result from instrument contamination as our CI-APi-TOF had never

341   been in contact with iodine (i.e. no nucleation experiments with iodine have yet been performed and no

342   iodide primary ions have been used). The observed signals could be assigned to IO_3^-, $(H_2O)IO_3^-$ and

343      $(HNO_3)IO_3^-$ (Table 1). To our knowledge the identification of iodine related peaks have not been

344   reported from measurements with a nitrate CIMS. However, Berresheim et al. (2000) reported the

345   presence of a peak at m/z 175 in the spectrum for the marine environment, which was not identified

346   previously but in the light of this study, can almost certainly be attributed to IO_3^-.

347   The diurnal pattern of IO_3^- and the related iodine peaks show a distinct pattern with a maximum

348   around noon following almost perfectly the diurnal pattern of sulfuric acid (Fig. 3). This may not be

349   surprising since the formation of HIO_3 is due to reaction between OIO and OH (Saiz-Lopez et al., 2012);

350   therefore, the iodic acid concentration is connected to the OH chemistry. After normalization of the

351   iodic acid signals with the nitrate primary ion count rates, a concentration of the neutral compound HIO_3

352   can be obtained by tentatively adopting the same calibration constant for iodic acid as for sulfuric acid.

353   Thereby a maximum average day-time concentration of $\sim3\times10^5$ molecule cm^{-3} can be found. Further

354   using the derived OH concentrations from the H_2SO_4 and CS measurements (Section 3.4) the derived

355   [HIO_3] can be used to estimate the concentration of OIO (Saiz-Lopez et al, 2012):

356

357      $$[\text{OIO}] = \frac{cs \cdot [\text{HIO}_3]}{k_{\text{OH+OIO}} \cdot [\text{OH}]}.$$ (5)

358

359   Equation (5) assumes that the only production channel of HIO_3 is the reaction between OH and OIO and

360   the only loss mechanism of HIO_3 is the uptake on aerosol. The reaction rate $k_{\text{OH+OIO}}$ can be taken from

361   the literature (Plane et al., 2006). In this way the concentration of OIO can be estimated to a typical

362   value of 5×10^6 molecule cm^{-3}, which is much lower than the values reported for the marine environment

363   (3 to 27 pptv, i.e. 7.5×10^7 to 6.8×10^8 molecule cm^{-3}, see Saiz-Lopez et al., 2012).

364   The relatively low values of [HIO_3] and [OIO] probably indicate that iodine chemistry is not very

365   important in terms of new particle formation at this site. This is supported by the fact that we could not

366 observe any clusters containing e.g. sulfuric acid and iodic acid or clusters containing more than one
367 iodine molecule. However, it is surprising that iodine can be detected more than 400 km away from the
368 nearest coast line. On the other hand, HYSPLIT back trajectory calculations (Stein et al., 2015) reveal
369 that in most cases the air was arriving from westerly directions and therefore had contact with the ocean
370 within the last 48 hours before arriving at the station. During the measurement period there was
371 unfortunately never a day where the air was clearly coming from easterly directions and had not been in
372 contact with the Atlantic Ocean or Mediterranean Sea within the previous days. Therefore, it could not
373 be checked if this would result in lower iodine signals. Despite the marine origin of the air masses
374 observed it is not clear how the iodine is transported over relatively large distances without being lost
375 on aerosol particles. If iodic acid is irreversibly lost on aerosol (similar to sulfuric acid) its lifetime
376 should only be on the order of several minutes at typical boundary layer conditions. Therefore, the
377 presence of iodine indicates either a local iodine source, or its transport from marine environments in
378 the form of a reservoir substance, e.g. CH_3I (the lifetime of CH_3I is in the order of 1 week, see Saiz-
379 Lopez et al., 2015), and subsequent release due to photolysis.

380 Regarding the sensitivity of the CI-APi-TOF it can be said that iodic acid (and, if present, probably
381 also its clusters) can be detected with high sensitivity. One aspect that helps in unambiguously
382 identifying iodic acid is the high negative mass defect of the iodine atom ($\Delta m \approx$ -0.1 Th). Furthermore,
383 this also contributes to the low detection limit for this compound because generally there will not be any
384 overlapping signals from other substances having the same integer mass (mass resolving power of the
385 instrument is ~4000 Th/Th, i.e. at m/z 175 the peak width at half maximum is ~0.04 Th). The method
386 introduced here therefore allows high-sensitivity measurement of $[HIO_3]$ as well as the estimation of
387 $[OIO]$ with the help of equation (5) in future studies. The lowest detectable concentrations should be
388 around 3×10^4 molecule cm^{-3}, or better, for $[HIO_3]$ and 5×10^5 molecule cm^{-3} (ca. 0.02 pptv) for $[OIO]$
389 when assuming the same calibration constant for HIO_3 as for H_2SO_4 and considering the lowest iodine
390 signal from Fig. 3.

391

392 **3.6 Amine, nitrosamine and ammonia measurements**

393

394 The detection of dimethylamine (DMA, $(CH_3)_2NH$) by means of nitrate chemical ionization with a CI-
395 APi-TOF has been described previously (Simon et al., 2016). The clustering between diethylamine
396 (DEA) and nitrate ion clusters has also been reported by Luts et al. (2011). The amines detected in the
397 present study include CH_5N (monomethylamine), C_2H_7N (dimethylamine, DMA or ethylamine, EA),
398 C_3H_9N (trimethylamine, TMA or propylamine, PA), $C_4H_{11}N$ (diethylamine, DEA) and $C_6H_{15}N$
399 (triethylamine, TEA). All these amines are identified as clusters in the CI-APi-TOF spectra where the
400 amines are associated both with the nitrate dimer $((amine)(HNO_3)NO_3^-)$ and the trimer
401 $((amine)(HNO_3)_2NO_3^-)$.

402 The high mass resolving power of the CI-APi-TOF allowed the identification of five different amines
403 (C1-, C2-, C3-, C4- and C6-amines, see above). Since the amines are all identified at two different
404 masses each (either with the nitrate dimer or the nitrate trimer) plotting the time series of each pair of
405 signals allows further verification of the amine signals since a different time trend would reveal that
406 another ion would interfer with the amine signal. This was sometimes the case when the relative
407 humidity was high and clusters of water and nitrate appeared with high water numbers. The cluster of
408 NO_3^- and 6 water molecules has a mass of 170.0518 Th and the C2-amine cluster $(C_2H_7N)(HNO_3)NO_3^-$
409 (170.0419 Th) cannot be separated from this primary ion cluster. Therefore, if large nitrate plus water
410 clusters were observed in the spectra, no C2-amine signal could be evaluated.

411 The same ion cluster chemistry applies for ammonia, which can also bind with the nitrate cluster
412 ions. Consequently, ammonia is detected as $(NH_3)(HNO_3)NO_3^-$ and $(NH_3)(HNO_3)_2NO_3^-$ (Table 1). To
413 our knowledge the existence of these cluster ions has not been reported previously.

414 In accordance with Simon et al. (2016) the cluster ion signals have been normalized by the following
415 relationship:

416

417 $$\text{amine}_{ncps} = \ln\left(1 + \frac{\{(\text{amine})(HNO_3)NO_3^-\} + \{(\text{amine})(HNO_3)_2NO_3^-\}}{\{(HNO_3)_2NO_3^-\}}\right),$$ (6)

418

419 where the curly brackets denote the count rates of the different ion clusters and the same formula can be
420 used when "amine" is replaced by NH_3 to obtain the normalized ammonia signal. The normalization
421 with the nitrate trimer has been chosen because we think that this is the dominant nitrate ion cluster the
422 amines (and ammonia) can bind to within the CI-APi-TOF ion reaction zone (Simon et al., 2016). Partial
423 evaporation of one HNO_3 from the resulting amine nitrate cluster within the CI-APi-TOF vacuum
424 chamber leads to the spread of the signal over the related masses separated by 62.9956 Th (HNO_3).

425 In addition, to the five amines mentioned before, we were able to identify dimethylnitrosamine
426 (NDMA, $(CH_3)_2NNO$) from its clusters $((CH_3)_2NNO)(HNO_3)NO_3^-$ and $((CH_3)_2NNO)(HNO_3)_2NO_3^-$
427 (Table 1). The signals from NDMA show a clear diurnal pattern on some days, which can be up to about
428 two orders of magnitude higher during the night compared to the day. This is in agreement with the
429 formation mechanism of NDMA via the reaction of DMA with OH and NO (Nielsen, Herrmann and
430 Weller, 2012). The lower concentrations during the day can be explained by the rapid photolysis rate of
431 NDMA (Nielsen, Herrmann and Weller, 2012). Since only C2-amines are capable of forming
432 nitrosamines no further nitrosamine could be identified from the mass spectra. Only a rough estimation
433 of the mixing ratio can be provided by using the calibration constant from Simon et al. (2016) which
434 was derived for DMA. Using this calibration constant the maximum mixing ratio of NDMA would be
435 ~100 pptv (or 2.5×10^9 molecule cm^{-3}). However, this value has a high uncertainty because no direct
436 calibration with NDMA was performed.

437 The average diurnal patterns of the four amines and ammonia are shown in Fig. 5. The data are an
438 average over 21 measurement days and the error bars represent one standard deviation. The temperature

439   profile is shown along with the CI-APi-TOF signals. The C4-, C6-amines and ammonia show a distinct
440   diurnal profile, which follows the temperature profile closely. The temperature-dependent signal
441   intensity could be due to partial re-evaporation of amines from the particulate phase. No correlation with
442   temperature is seen for the C1-, C2- and C3-amines, which could indicate efficient stabilization of these
443   amines in the particulate phase due to acid-base reactions (Kirkby et al., 2011; Almeida et al., 2013).

444   No direct calibration for amines, NDMA and ammonia was performed during the campaign.
445   Therefore, only a rough estimation of the mixing ratios can be made. Using the calibration curve for
446   DMA by Simon et al. (2016), 1×10^{-4} ncps (normalized counts per second) correspond to ~1 pptv of
447   DMA. With this conversion the average mixing ratios are between about 1 and 5 pptv for the amines.
448   The mixing ratios from this study are in a similar range as those reported from measurements in a
449   southeastern US forest (You et al., 2014) but generally lower as those from three different sites in the
450   US (Freshour et al., 2014).

451   The ncps for ammonia are lower than for the amines, which should not be the case if the sensitivity
452   towards ammonia and amines would be the same because the ammonia mixing ratios are almost
453   certainly higher than the ones for the amines in this environment. The ammonia mixing ratio can be
454   above several ppbv in rural areas (von Bobrutzki et al., 2010). Therefore, the sensitivity of the nitrate
455   CI-APi-TOF towards ammonia seems to be significantly lower than for amines. This is reasonable, since
456   other studies found that acid-base clusters between sulfuric acid (including the bisulfate ion) and amines
457   are much more stable compared to sulfuric acid ammonia clusters (Kirkby et al., 2011; Almeida et al.,
458   2013). Therefore, the acid base clustering between nitric acid (including the nitrate ion) and ammonia
459   or amines could follow a similar rule, which would lead to faster evaporation of the ammonia nitrate
460   clusters. For this reason only the relative signals for ammonia can be used at the moment without
461   providing estimated mixing ratios.

462   Recently it has been suggested that diamines could play an important role in ambient NPF (Jen et al.,
463   2016a); however, we could not identify diamines from the high-resolution mass spectra.

464

465   **3.7 Sulfuric acid dimer**

466

467   Occasionally, the CI-APi-TOF sulfuric acid dimer signal was above background levels. The dimer
468   ($(H_2SO_4)HSO_4^-$) was identified from the high resolution spectra on nine campaign days. The measured
469   sulfuric acid dimer concentrations are shown as a function of the sulfuric acid monomer concentrations
470   in Fig. 6. For comparison, CLOUD chamber data from nucleation experiments in the ternary sulfuric
471   acid-water-dimethylamine system are included (red circles in Fig. 6, Kürten et al., 2014). In addition,
472   the lower dashed line shows the expected dimer formation due to ion-induced clustering (IIC) of sulfuric
473   acid monomers in the CI-APi-TOF ion reaction zone (Hanson and Eisele, 2002; Zhao et al., 2010).

474   The data indicate that the measured dimer concentrations are clearly above the background level set
475   by ion-induced clustering. On the other hand the concentrations are lower than what has been measured

13

476 in CLOUD for kinetic nucleation in the sulfuric acid-water-dimethylamine system at 5°C and 38% RH

477 (Almeida et al., 2013; Kürten et al., 2014). Clearly, the neutral sulfuric acid dimers were stabilized by a

478 ternary compound, otherwise their concentrations would not have been measurable at these relatively

479 warm conditions because the dimer (without a ternary compound) evaporation rate is quite high ($> 10^5$

480 s^{-1} at 290 K, Hanson and Lovejoy, 2006; Kürten et al., 2015). On the other hand the ternary stabilizing

481 agent evaporates after charging of the sulfuric acid dimers because no cluster between the sulfuric acid

482 dimer and another compound (besides HNO_3 from the ion source) could be identified. This means that

483 although the dimers contained at least one additional molecule in the neutral state, the ionized dimer

484 will be detected as $(H_2SO_4)HSO_4^-$ (Ortega et al., 2014; Jen et al., 2014), which makes it impossible to

485 identify the stabilizing agent. Only when larger clusters of sulfuric acid are present (trimer and larger)

486 stabilizing agents like ammonia or amines can stay in the cluster after charging with the nitrate ion (Zhao

487 et al., 2011; Kirkby et al., 2011; Ortega et al., 2014; Kürten et al., 2014). Unfortunately, no large sulfuric

488 acid clusters (trimer and larger) were measurable during the campaign, probably because their

489 concentrations were too low. Therefore, only speculations about the stabilizing agent responsible for the

490 high dimer concentrations can be made. It is quite unlikely that ammonia would be the only stabilizing

491 compound for the dimers since previous studies have shown that the relatively high dimer concentration

492 measured at rather low sulfuric acid monomer concentrations ($< 2\times10^7$ molecule cm^{-3}) cannot be

493 explained by sulfuric acid-ammonia-water nucleation (Hanson and Eisele, 2002; Jen et al., 2014). In

494 addition, efficient clustering between sulfuric acid and iodic acid can probably be ruled out (provided

495 that these compounds would be capable of producing a cluster with a low evaporation rate) as the

496 concentrations of iodic acid are quite low ($\sim 3\times10^5$ molecule cm^{-3} at maximum, see Section 3.5). This

497 means that the arrival rate of iodic acid on a sulfuric acid dimer is on the order of 10^{-4} s^{-1} (using a

498 collision rate of 5×10^{-10} cm^3 molecule^{-1} s^{-1}). Due to the high evaporation rate of the pure sulfuric acid

499 dimer no significant dimer stabilization by iodic acid can be expected.

500 Whether amines are responsible for the dimer formation in the present study cannot be concluded. If

501 they were, the lower dimer concentrations compared to the CLOUD chamber results (Kürten et al.,

502 2014) could be attributed to the higher temperatures in the present study, which result in faster

503 evaporation rates. Another explanation would be the lower amine mixing ratios. In the CLOUD study

504 dimethylamine was present at 10 pptv, or higher. In addition, it cannot be concluded that e.g. the

505 measured C2-amines are all dimethylamine, if a significant fraction of them were, e.g., ethylamine, its

506 stabilizing effect could be significantly lower. This remains somewhat speculative as no data regarding

507 NPF from ethylamine and sulfuric acid was found, however, triethylamine was reported to have a

508 relatively weak effect on nucleation compared to DMA or TMA (Glasoe et al., 2015). Other compounds

509 which are present and have been shown to form new particles are HOM (Schobesberger et al., 2013;

510 Ehn et al., 2014; Riccobono et al., 2014;) although their stabilizing effect on neutral sulfuric acid dimers

511 remains to be elucidated.

512   Regarding the observations shown in Fig. 6, it should be noted that no ion filter (high voltage electric

513   field in the CI-APi-TOF inlet to remove ambient ions) was used in the present study. This could in

514   principle lead to the detection of ambient ions and clusters, which did not undergo charging in the CI-

515   APi-TOF ion reaction zone. If this were the case, no representative concentrations of the corresponding

516   neutral sulfuric acid dimer would be derived. CLOUD studies reported that charged sulfuric acid

517   monomers (HSO_4^-) and dimers ((H_2SO_4)HSO_4^-) could be observed with a different nitrate chemical

518   ionization mass spectrometer (CIMS) under some conditions (Rondo et al., 2014; Kürten et al., 2015).

519   However, for ambient measurements, no significant effect could be observed for sulfuric acid monomers

520   (Rondo et al., 2014). In principle, the sulfuric acid dimer could be more strongly affected by the

521   detection of ambient ions since the neutral dimer concentration is much lower than the sulfuric acid

522   monomer, while the negative ambient ion spectrum can be dominated by the charged sulfuric acid dimer

523   (Eisele et al., 2006). Therefore, we cannot entirely rule out that ambient ions had some effect on the data

524   shown in Fig. 6. However, the ambient ions would need to overcome an electric field before they could

525   enter the ion reaction zone (Kürten et al., 2011; Rondo et al., 2014). In the CIMS and the CI-APi-TOF

526   a negative voltage is used to focus the primary ions to the center of the reaction zone, while the sample

527   line is electrically grounded. This means negative ambient ions would need to overcome a repulsing

528   electric field which acts as a barrier. Light ions will be efficiently deflected due to their high mobility

529   but heavier ions can in principle penetrate more easily. Consequently, CIMS measurements at the

530   CLOUD chamber showed that the apparent dimer signal measured by the CIMS correlated with large

531   ion clusters (pentamer, i.e. (H_2SO_4)$_4HSO_4^-$ and larger, which underwent subsequent fragmentation) but

532   not with the (H_2SO_4)HSO_4^- signal; the charged clusters were measured simultaneously with an APi-

533   TOF (Junninen et al., 2010; Kürten et al., 2015). The CI-APi-TOF used in this study utilized a higher

534   voltage for the ion focusing compared to the CIMS (ca. -500 V instead of -220 V in the CIMS) and

535   should therefore prevent smaller masses even more efficiently from entering the ion source than in the

536   study by Kürten et al. (2015). In addition, the absence of any trimer signal ((H_2SO_4)$_2HSO_4^-$) in the

537   spectra argues against ambient ion detection. In a previous study by Eisele et al. (2006) ambient ion

538   measurements showed, besides signals for (H_2SO_4)HSO_4^-, also signals for (H_2SO_4)$_2HSO_4^-$ which were

539   on average ~50% of the dimer signals. Since the CI-APi-TOF design, with its repulsing voltages towards

540   ambient ions in the ion reaction zone, should be more sensitive towards the trimer than towards the

541   dimer, the absence of sulfuric acid trimer signals argues against a significant bias in the data due to

542   charged ambient clusters.

543

544   **3.8 Highly oxidized organic molecules (HOM)**

545

546   Recently, the rapid autoxidation of atmospherically relevant organic molecules, such as isoprene and

547   monoterpenes, was described (Crounse et al., 2013; Ehn et al., 2014). There is evidence that these HOM

548   are involved in the formation of secondary aerosol and can even promote the formation of new aerosol

549   particles (Jokinen et al., 2015; Kirkby et al., 2016). Nitrate chemical ionization mass spectrometry is

550   capable of detecting a suite of HOM when the O:C-ratio is high (e.g. > ~0.6 for C10 and > ~0.35 for

551   C19/C20 compounds) through association of an NO_3^- primary ion (Ehn et al., 2014), while other

552   ionization techniques are more selective towards less oxidized compounds (Aljawhary et al., 2013).

553   Many recent publications report peak lists for different compounds identified from chamber or ambient

554   measurements with nitrate chemical ionization (Ehn et al., 2012; Kulmala et al., 2013; Ehn et al., 2014;

555   Mutzel et al., 2015; Praplan et al., 2015; Jokinen et al., 2015; Kirkby et al., 2016). The species from the

556   previous studies are mainly C10 (containing 10 carbon atoms) or C20 (containing 19 or 20 carbon atoms)

557   compounds originating from reactions between monoterpenes (in most cases from α-pinene) and ozone

558   and/or OH.

559   The C10 compounds can be further segregated in HOM radicals (RO_2, i.e. $C_{10}H_{15}O_{i\geq6}$), HOM

560   monomers ($C_{10}H_{14}O_{i\geq7}$ and $C_{10}H_{16}O_{i\geq6}$) and HOM involving reactions with nitrate ($C_{10}H_{15}NO_{i\geq7}$ and

561   $C_{10}H_{16}N_2O_{i\geq8}$) (Jokinen et al., 2014). Dimers (C19/C20 compounds) originate from reactions among

562   HOM RO_2 radicals (Ehn et al., 2014).

563   The spectra were evaluated according to the peak list shown in Table 2 regarding HOM. It should be

564   noted that the listed compounds represent some fraction of the observed signal in the monomer and

565   dimer region although not all of the peaks that are present are identified yet. Figure 7 shows a comparison

566   between the average day time and the average night time spectra for the mass to charge range between

567   m/z 300 and 650. According to Fig. 7 the main difference between day and night are the significantly

568   higher signals in the dimer region during the night.

569   Fig. 8 shows the diurnal variation of the HOM (separated into HOM radicals, HOM monomers, HOM

570   nitrates and HOM dimers according to Table 2) together with other parameters (NO, NO_2, O_3 and global

571   radiation). One striking feature is the pronounced maximum concentration of HOM dimers during the

572   night. During the day when the global radiation shows values above zero the dimer signals drop by about

573   one order of magnitude and reach levels, which are close to the detection limit of the instrument. The

574   low day-time dimer concentrations are probably due to enhanced NO, HO_2 and $R'O_2$ concentrations

575   during the day. These compounds can react with HOM RO_2 radicals and thereby inhibit the formation

576   of dimers; which are a result of the reaction between two RO_2 radicals. As can be seen from Fig. 8 the

577   NO concentration peaks in the morning. HO_2 was not measured but typically peaks around noon or in

578   the later afternoon (Monks, 2005). Direct photolysis of HOM dimers has to our knowledge not been

579   reported in the literature but could in principle also explain the dimer pattern seen in Fig. 8.

580   The HOM monomer signal (Fig. 8) does not show a pronounced diurnal cycle, only in the early

581   morning the signals are reduced by about 50% compared to the daily average. Slightly higher values

582   around noon could be explained by the higher O_3 and OH concentrations during mid-day, which lead to

583   enhanced formation of HOM through reactions between these compounds and monoterpenes (Jokinen

584   et al., 2015; Kirkby et al., 2016). The HOM nitrates, di-nitrates and radicals show almost the same

585   profile as the HOM monomers. This might be expected for the HOM radicals as these can be regarded

as the precursors for the HOM monomers but the fact that the HOM nitrates follow an almost identical pattern is somewhat surprising as the NO mixing ratio shows a different profile and is thought to be involved in the formation of the HOM nitrates. However, further involvement of e.g. OH, HO$_2$ and R'O$_2$ in the HOM formation should also play a role and therefore influence their diurnal pattern. The elucidation of the HOM formation mechanisms is beyond the scope of this article and will therefore not be discussed further. More field and chamber experiments are needed to identify the influence of different trace gases and radicals on the formation and concentration of HOM.

3.9 Particle formation rates

The presence of small particles (< ~20 nm) was observed on almost every day during the campaign. However, often nanometer-sized particles appeared suddenly without clear growth from the smallest size the nDMA covered (slightly above 3 nm). In total there were seven events where clear growth was detectable and these events were the only ones for which a new particle formation rate (J) was derived. It should be noted that clear NPF was observed only on 6 days, however, for one day two NPF rates were derived, which results in a total of 7 NPF rates.

In accordance with other previous studies (Metzger et al., 2010; Kirkby et al., 2011) we have first derived a new particle formation rate at a larger mobility diameter d_{p2} (2.5 nm in the present study), which was corrected to a smaller diameter of $d_{p1} = 1.7$ nm in a second step. The formation rate J_{dp2} is obtained from the time derivative of the small particle concentration, which follows from the difference in particle concentrations ($N_{2.5-10}$) measured by the TSI 3776 (cut-off diameter of 2.5 nm) and a TSI 3010 (cut-off diameter of 10 nm):

$$J_{d_{p2}} = \frac{dN_{2.5-10}}{dt} + CS_{d_{p2}} \cdot N_{2.5-10} + \frac{GR}{10nm-2.5nm} \cdot N_{2.5-10}. \tag{7}$$

The second term on the right-hand side in equation (7) accounts for the loss of small particles on particles larger than 2.5 nm, while the third term accounts for the growth of particles out of the size range under consideration (Kulmala et al., 2012). The coagulation sink CS_{dp2} is calculated from the particle size distribution measured by the nDMA and the SMPS. The second step involves an exponential correction to obtain the particle formation rate at the smaller size, J_{dp1}, by taking into account the coagulation sink and the growth rate (GR) of particles (Lehtinen et al., 2007):

$$J_{d_{p1}} = J_{d_{p2}} \cdot exp\left(\frac{CS_{d_{p1}}}{GR} \cdot dp_1 \cdot \gamma\right). \tag{8}$$

The factor γ is defined as follows (Lehtinen et al., 2007):

622 $$\gamma = \frac{1}{s+1} \cdot \left(\left(\frac{d_{p2}}{d_{p1}} \right)^{s+1} - 1 \right), \qquad (9)$$

623

624 where s is the slope of the coagulation sink as a function of size for the size range between d_{p1} and d_{p2}

625 ($s = \log(CS_{dp2}/CS_{dp1})/\log(d_{p2}/d_{p1})$). The value of s can be derived from the measured particle size

626 distribution and was found to be around -1.6 for the present study, which is in good agreement with the

627 values reported by Lehtinen et al. (2007). The growth rate was derived from the nDMA measurements

628 in the size range between 3 and 10 nm by fitting a Gaussian function to the particle size distribution to

629 determine the mode diameter for all measured size distributions. Applying a linear fit to the mode

630 diameter as a function of time yields the GR used in equation (8) (Hirsikko et al., 2005). Errors are

631 calculated by taking into account the statistical variation of the particle formation rates J_{dp2} as well as

632 systematic errors on GR (factor of 2), d_{p2} (factor 1.3) and CS (factor 1.5).

633   Figure 9 shows a comparison between J_{dp1} from this study, data from other field studies and formation

634 rates from CLOUD chamber studies for the system of sulfuric acid, dimethylamine and water at 278 K

635 (Almeida et al., 2013) as well as for oxidized organic compounds with sulfuric acid and water

636 (Riccobono et al., 2014).

637

638

639 **4. Discussion**

640

641 By comparing time periods where significant new particle formation (NPF) occurred to time periods

642 where no NPF was observed, some conclusions can be drawn about the relevance of certain parameters

643 regarding NPF. Figure 10 shows a comparison for a variety of parameters by comparing nucleation days

644 to no nucleation days (red bars) and periods with high sulfuric acid dimer concentrations to no nucleation

645 days when there are also no high dimer concentrations (blue bars).

646   It is evident from Fig. 10 that sulfuric acid is on average a factor of 2 to 2.5 higher on days with

647 nucleation; although the variability is rather high (error bars take into account the standard deviations

648 of a parameter both for the nucleation days and the no nucleation days). The enhanced sulfuric acid

649 concentrations confirm the importance of this compound regarding NPF, which has also been shown in

650 numerous other studies (e.g. Weber et al., 1997; Kulmala et al., 2004; Fiedler et al., 2005; Kuang et al.,

651 2008). The OH concentration and the global radiation are also enhanced during nucleation, which is not

652 surprising given the fact that the parameters H_2SO_4, OH and global radiation are connected. The relative

653 humidity is generally lower during nucleation periods, which has also been reported in previous studies

654 (Hamed et al., 2011; Nieminen et al., 2015).

655   Regarding amines and ammonia Fig. 10 reveals an anti-correlation between their concentration and

656 the occurrence of NPF or sulfuric acid dimer formation (factor 2 to 5 lower during nucleation). However,

657 this does not necessarily mean that these compounds inhibit the formation of particles. On the contrary,

18

658   it could mean that amines and ammonia are efficiently taken up by small clusters and therefore are also

659   involved in the formation of new particles. Unlike sulfuric acid, amines and ammonia are not produced

660   in the gas phase and therefore their concentration will decrease with increasing distance from their

661   sources depending on the condensation sink. During nucleation the condensation sink is slightly

662   enhanced (Fig. 10), probably because of the newly formed particles. However, the CS is only calculated

663   for particles larger than 3 nm. Also smaller particles and sulfuric acid clusters can contain amines

664   (Kürten et al., 2014) and even the sulfuric acid monomer can be bound to dimethylamine (Ortega et al.,

665   2012; Kürten et al., 2014). Therefore, continuous production of sulfuric acid and its clusters will lead to

666   a depletion of amines away from their sources, although no mixed clusters of sulfuric acid and amines

667   could be observed; this is probably the case because their concentrations were too low to be measured

668   with the CI-APi-TOF. As sulfuric acid concentrations are high during nucleation this could explain the

669   low amine values. Efficient uptake of amines in the particle phase has also been reported in a previous

670   field study (You et al., 2014). In addition, the limited pool of amines can also be the explanation for the

671   relatively low slope from Fig. 6 (sulfuric acid dimer vs. monomer) for some of the periods with elevated

672   sulfuric acid dimer concentrations. If the sulfuric acid concentration increases, the ratio of the free

673   (unbound) amine to sulfuric acid concentration drops, and there are fewer amines available to stabilize

674   the sulfuric acid dimers. This is a different situation compared to the CLOUD experiment where the

675   amine to sulfuric acid concentration was maintained at a ratio of ~100 over the entire duration of the

676   experiments. However, from these observations we cannot unambiguously conclude if the amines are

677   involved in the very first steps of nucleation, or if they are depleted due to clusters, which do not need

678   the help of amines in order to nucleate. One other aspect that could explain the low amine ratios is the

679   somewhat enhanced OH concentration during the nucleation days, as amines react with OH. However,

680   the life-time of amines regarding their reactions with OH is on the order of hours (Ge et al., 2011),

681   whereas the uptake on particles is significantly faster (if CS is on the order of 10^{-3} to 10^{-2} s^{-1}).

682   Regarding the possibility that sulfuric acid and amines can explain the observed nucleation it has to

683   be noted that no clusters involving more than two sulfuric acid molecules could be observed. In the

684   following we will calculate the maximum expected sulfuric acid trimer concentration and discuss what

685   parameters can lower this concentration. The maximum measured sulfuric acid dimer concentration is

686   around 1×10^5 molecule cm^{-3} for a sulfuric acid monomer concentration of 1×10^7 molecule cm^{-3}. A

687   sulfuric acid trimer will be formed through the collision between a monomer and a dimer (collision rate

688     $K_{1,2}$), whereas the loss rate of the trimer is defined by the sum of the condensation sink (CS) and its

689   evaporation rate ($k_{e,3}$). At steady-state this would yield the following equation for the trimer

690   concentration N_3 as function of the monomer and dimer concentrations N_1 and N_2 (for simplicity this

691   neglects a potential contribution from tetramer evaporation):

692

693     $$N_3 = \frac{K_{1,2} \cdot N_1 \cdot N_2}{CS + k_{e,3}}. \tag{10}$$

694

695 Using a value of 5×10^{-10} molecule^{-1} cm^3 s^{-1} for $K_{1,2}$ and a condensation sink (CS) of 5×10^{-3} s^{-1} for the
696 above mentioned monomer and dimer concentrations would yield a trimer concentration of 1×10^5
697 molecule cm^{-3} if the trimer evaporation rate would be zero. This concentration should be detectable with
698 our CI-APi-TOF. The fact that we do not see the trimer could indicate that the trimer evaporation rate
699 is non-zero. For a high amine to sulfuric acid ratio nucleation proceeds at or close to the kinetic limit
700 (Jen et al., 2014; Kürten et al., 2014). However, if the amine concentration is not very high, not every
701 trimer that is formed would be stable (as it is the case for a favored acid-base ratio, see Ortega et al.,
702 2012) and therefore could evaporate rapidly. This would result in lower trimer concentrations, which
703 could be below the detection limit of the CI-APi-TOF. From this perspective the absence of larger
704 sulfuric acid amine clusters is not necessarily an indication that this system is not responsible for new
705 particle formation. In other regions where the sulfuric acid and amine mixing ratios are even higher (i.e.
706 very close to amine sources) such clusters can be observable (Zhao et al., 2011). Recently, Jen et al.
707 (2016b) provided evidence that nitrate chemical ionization could not be sensitive towards sulfuric acid-
708 amine or sulfuric acid-diamine clusters if these contain three or more sulfuric acid molecules because
709 of the lowered acidity of such clusters by the basic amines/diamines. This could also explain the absence
710 of clusters beyond the dimer in the present study. Further measurements using different primary ions
711 are needed to investigate this possibility further.

712   The C10 and C20 signals for NPF and no nucleation days are not significantly different (Fig. 10).
713 This can be interpreted in different ways: (1) the HOM are not important in terms of NPF, (2) HOM are
714 generally high enough and it needs just enough sulfuric acid to initiate nucleation involving HOM, or
715 (3) „HOM" is too broadly defined and only a subgroup of HOM is involved in the nucleation but
716 currently we cannot distinguish this group. Neither of the possibilities can be proven right or wrong.
717 However, what can be said is that it is unlikely that the identified HOM alone are capable of producing
718 new particles to a significant extent at the conditions of the present study. The HOM dimer
719 concentrations (Fig. 8) are significantly higher during the night than during the day. Nevertheless, no
720 night-time nucleation is observed. This could be interpreted as an indication that if HOM are involved
721 in NPF it requires additional compounds such as sulfuric acid to initiate significant nucleation.
722 Alternative explanations for the absence of night time nucleation could be the suppression of the
723 formation of HOM that can nucleate by NO$_3$ during the night, or low [OH], which is required for the
724 formation of nucleating HOM.

725   Kulmala et al. (2013) proposed that $C_{10}H_{15}NO_8$ (detected as a cluster with NO$_3^-$ at 339.0681 Th)
726 could be important because NPF correlated even better with this compound compared to sulfuric acid.
727 During nucleation days this compound is only slightly elevated (Fig. 10) and this could be due to the
728 generally higher OH levels although the exact formation mechanism of $C_{10}H_{15}NO_8$ has to our knowledge
729 not been reported yet. During nucleation, no mixed clusters between sulfuric acid and HOM could be
730 identified. However, this also does not rule out their existence as the concentrations could be below the

CI-APi-TOF detection limit, or a low charging efficiency with the nitrate primary ion could prevent their detection. Furthermore, not all signals are identified yet.

The observed particle formation rates (Fig. 9) are consistent with the rates observed at other sites, although being at the upper end of the typical ranges that have been previously measured. The present data seem to agree a bit better to CLOUD chamber data for the system of sulfuric acid, water and dimethylamine (Almeida et al., 2013) compared to data for the system of sulfuric acid, water and oxidized organics from pinanediol (Riccobono et al., 2014). However, a direct comparison is difficult as the conditions between this ambient study and the CLOUD chamber experiments are not identical (with respect to T, RH, CS, amine mixing ratios, HOM concentrations, etc.).

5. Summary

In spring 2014 (May 18 to June 7) a field campaign was conducted at a rural site in central Germany (Vielbrunn/Odenwald). The measurement site was in proximity (within 450 to 1100 m distance) of three larger dairy farms. The perspective of this campaign was to evaluate if there is a connection between new particle formation and the concentration of amines and/or ammonia. Furthermore, the impact of highly oxidized organic molecules (HOM) from surrounding forests was investigated. A nitrate Chemical Ionization-Atmospheric Pressure interface-Time Of Flight mass spectrometer (CI-APi-TOF) was used to identify gas-phase compounds and clusters. Particle counters and differential mobility analyzers were used to characterize the aerosol size distribution and number density. The following conclusions can be drawn from our measurements:

- Nitrate CI-APi-TOF can be used to measure sulfuric acid, iodic acid, amines, a nitrosamine, ammonia and HOM; the measurement of iodic acid, ammonia and the nitrosamine has not been described before; the method is therefore even more versatile than previously thought and well suited to study all of the above-mentioned compounds during field measurements.
- The sulfuric acid concentration can be well described by proxies (SO_2, global radiation, RH and CS or just by SO_2 and global radiation) for this site with a similar accuracy as reported in a previous study (Mikkonen et al., 2011).
- Significant sulfuric acid dimer concentrations were measured; it is, however, not clear what compound stabilizes the neutral dimers; larger sulfuric acid clusters (trimer and beyond) were not observed.
- Amines (C1-, C2-, C3-, C4- and C6-amines) are present at estimated mixing ratios between approximately 1 and 5 pptv, which is consistent with other studies; the C4- and C6-amines as well as ammonia show a diurnal variation, which follows the temperature profile.
- Iodine has been observed (probably iodic acid) on every day, somewhat surprising for a continental site located more than 400 km away from the ocean; the nitrate CI-APi-TOF has a

768 high sensitivity towards iodic acid and its presence indicates long-range transport of iodine
769 containing substances (although a local source cannot entirely be ruled out); using OH
770 concentrations also OIO concentrations can be estimated; however, both [HIO_3] (~3×10^5
771 molecule cm^{-3}) and [OIO] (~5×10^6 molecule cm^{-3}) are probably too low to affect new particle
772 formation significantly at this site.

773 • The diurnal pattern of HOM dimers shows maximum concentrations during the night but no night
774 time nucleation is observed; the day time concentration could be low due to the presence of NO
775 and/or HO_2 which suppress the HOM dimer formation.

776 • Relatively high particle formation rates are found, which are rather at the upper end of the
777 atmospheric observations for other rural sites; the rates are compatible with CLOUD chamber
778 data both for the systems of sulfuric acid, water and dimethylamine (Almeida et al., 2013), as well
779 as for a system involving sulfuric acid, water and oxidized organics (Riccobono et al., 2014); no
780 definitive answer can be given which system is more relevant.

781 • Nucleation seems to be favored on days with relatively low RH and high sulfuric acid; an anti-
782 correlation with the amine and ammonia signals is observed, this could be due to efficient uptake
783 of these compounds on clusters and particles during NPF as amines and ammonia are not
784 produced in the gas-phase.

785 The above bullet points seem to support recent findings about the relevance of amines in terms of NPF
786 and early growth (Chen et al., 2012; Almeida et al., 2013; Kulmala et al., 2013; Lehtipalo et al., 2016).
787 However, it cannot be unambiguously concluded that amines are more relevant for NPF than HOM at
788 this site because no nucleating clusters could be directly observed. More studies like the present one are
789 necessary in the future to obtain better statistics about the parameters relevant for NPF (Fig. 10). Ideally,
790 such measurements should include further instrumentation including a PSM (Vanhanen et al., 2011) for
791 the measurement of clusters and small particles (< 3 nm), an APi-TOF (Junninen et al., 2010) for
792 identification of charged nucleating clusters, an instrument for HO_x/RO_x measurements (Mauldin et al.,
793 2016) and an instrument for sensitive amine measurements capable of speciating the amines.

800   **References**

801

802   Aljawhary, D., Lee, A. K. Y., and Abbatt, J. P. D.: High-resolution chemical ionization mass
803   spectrometry (ToF-CIMS): application to study SOA composition and processing, Atmos. Meas. Tech.,
804   6, 3211–3224, doi: 10.5194/amt-6-3211-2013, 2013.

805

806   Almeida, J., Schobesberger, S., Kürten, A., Ortega, I. K., Kupiainen-Määttä, O., Praplan, A. P., Adamov,
807   A., Amorim, A., Bianchi, F., Breitenlechner, M., David, A., Dommen, J., Donahue, N. M., Downard,
808   A., Dunne, E. M., Duplissy, J., Ehrhart, S., Flagan, R. C., Franchin, A., Guida, R., Hakala, J., Hansel,
809   A., Heinritzi, M., Henschel, H., Jokinen, T., Junninen, H., Kajos, M., Kangasluoma, J., Keskinen, H.,
810   Kupc, A., Kurtén, T., Kvashin, A. N., Laaksonen, A., Lehtipalo, K., Leiminger, M., Leppä, J., Loukonen,
811   V., Makhmutov, V., Mathot, S., McGrath, M. J., Nieminen, T., Olenius, T., Onnela, A., Petäjä, T.,
812   Riccobono, F., Riipinen, I., Rissanen, M., Rondo, L., Ruuskanen, T., Santos, F. D., Sarnela, N.,
813   Schallhart, S., Schnitzhofer, R., Seinfeld, J. H., Simon, M., Sipilä, M., Stozhkov, Y., Stratmann, F.,
814   Tomé, A., Tröstl, J., Tsagkogeorgas, G., Vaattovaara, P., Viisanen, Y., Virtanen, A., Vrtala, A., Wagner,
815   P. E., Weingartner, E., Wex, H., Williamson, C., Wimmer, D., Ye, P., Yli-Juuti, T., Carslaw, K. S.,
816   Kulmala, M., Curtius, J., Baltensperger, U., Worsnop, D. R., Vehkamäki, H., and Kirkby, J.: Molecular
817   understanding of sulphuric acid-amine particle nucleation in the atmosphere, Nature, 502, 359–363, doi:
818   10.1038/nature12663, 2013.

819

820   Berndt, T., Jokinen, T., Sipilä, M., Mauldin III, R. L. Herrmann, H., Stratmann, F., Junninen, H., and
821   Kulmala, M: H_2SO_4 formation from the gas-phase reaction of stabilized Criegee Intermediates with SO_2:
822   Influence of water vapour content and temperature, Atmos. Env., 89, 603–612, doi:
823   10.1016/j.atmosenv.2014.02.062, 2014.

824

825   Berresheim, H., Elste, T., Plass-Dülmer, C., Eisele, F. L., and Tanner, D. J.: Chemical ionization mass
826   spectrometer for long-term measurements of atmospheric OH and H_2SO_4, Int. J. Mass Spectrom., 202,
827   91–109, doi: 10.1016/S1387-3806(00)00233-5, 2000.

828

829   Bianchi, F., Tröstl, J., Junninen, H., Frege, C., Henne, S., Hoyle, C. R., Molteni, U., Herrmann, E.,
830   Adamov, A., Bukowiecki, N., Chen, X., Duplissy, J., Gysel, M., Hutterli, M., Kangasluoma, J.,
831   Kontkanen, J., Kürten, A., Manninen, H. E., Münch, S., Peräkylä, O., Petäjä, T., Rondo, L., Williamson,
832   C., Weingartner, E., Curtius, J., Worsnop, D. R., Kulmala, M., Dommen, J., and Baltensperger, U.: New
833   particle formation in the free troposphere: A question of chemistry and timing, Science, 352, 1109–
834   1112, doi: 10.1126/science.aad5456, 2016.

835

836   Blake, R. S., Monks, P. S., and Ellis, A. M.: Proton-Transfer Reaction Mass Spectrometry, Chem. Rev.,
837   109, 861–896, doi: 10.1021/cr800364q, 2009.

838

839   Boy, M., Mogensen, D., Smolander, S., Zhou, L., Nieminen, T., Paasonen, P., Plass-Dülmer, C., Sipilä,
840   M., Petäjä, T., Mauldin, L., Berresheim, H., and Kulmala, M.: Oxidation of SO_2 by stabilized Criegee
841   intermediate (sCI) radicals as a crucial source for atmospheric sulfuric acid concentrations, Atmos.
842   Chem. Phys., 13, 3865–3879, doi: 10.5194/acp-13-3865-2013, 2013.

843

844   Cappellin, L., Karl, T., Probst, M., Ismailova, O., Winkler, P. M., Soukoulis, C., Aprea, E., Märk, T. D.,
845   Gasperi, F., and Biasioli, F.: On quantitative determination of volatile organic compound concentrations
846   using proton transfer reaction time-of-flight mass spectrometry, Env. Sci. Technol., 46, 2283–2290, doi:
847   10.1021/es203985t, 2012.

848

849   Chang, D., Song, Y., and Liu, B.: Visibility trends in six megacities in China 1973–2007, Atmos. Res.,
850   94, 161–167, doi: 10.1016/j.atmosres.2009.05.006, 2009.

851

852   Chen, M., Titcombe, M., Jiang, J., Jen, C., Kuang, C., Fischer, M. L., Eisele, F. L., Siepmann, J. I.,
853   Hanson, D. R., Zhao, J., and McMurry, P. H.: Acid–base chemical reaction model for nucleation rates
854   in the polluted atmospheric boundary layer, P. Natl. Acad. Sci. USA, 109, 18713–18718, doi:
855   10.1073/pnas.1210285109, 2012.

856

857   Crounse, J. D., Nielsen, L. B., Jørgensen, S., Kjaergaard, H. G., and Wennberg, P. O.: Autooxidation of
858   organic compounds in the atmosphere, J. Phys. Chem. Lett., 4, 3513–3520, doi: 10.1021/jz4019207,
859   2013.

860

861   Ehn, M., Kleist, E., Junninen, H., Petäjä, T., Lönn, G., Schobesberger, S., Dal Maso, M., Trimborn, A.,
862   Kulmala, M., Worsnop, D. R., Wahner, A., Wildt, J., and Mentel, Th. F.: Gas phase formation of
863   extremely oxidized pinene reaction products in chamber and ambient air, Atmos. Chem. Phys., 12,
864   5113–5127, doi: 10.5194/acp-12-5113-2012, 2012.

865

866   Ehn, M., Thornton, J. A., Kleist, E., Sipilä, M., Junninen, H., Pullinen, I., Springer, M., Rubach, F.,
867   Tillmann, R., Lee, B., Lopez-Hilfiker, F., Andres, S., Acir, I.-H., Rissanen, M., Jokinen, T.,
868   Schobesberger, S., Kangasluoma, J., Kontkanen, J., Nieminen, T., Kurtén, T., Nielsen, L. B., Jørgensen,
869   S., Kjaergaard, H. G., Canagaratna, M., Dal Maso, M., Berndt, T., Petäjä, T., Wahner, A., Kerminen,
870   V.-M., Kulmala, M., Worsnop, D. R., Wildt, J., and Mentel, T. F.: A large source of low-volatility
871   secondary organic aerosol, Nature, 506, 476–479, doi: 10.1038/nature13032, 2014.

872

873 Eisele, F. L., and Tanner, D. J.: Measurement of the gas phase concentration of H_2SO_4 and methane

874 sulfonic acid and estimates of H_2SO_4 production and loss in the atmosphere, J. Geophys. Res., 98, D5,

875 9001–9010, doi: 10.1029/93JD00031, 1993.

876

877 Eisele, F. L., Lovejoy, E. R., Kosciuch, E., Moore, K. F., Mauldin III, R. L., Smith, J. N., McMurry, P.

878 H., and Iida, K.: Negative atmospheric ions and their potential role in ion-induced Nucleation, J.

879 Geophys. Res., 111, D04305, doi: 10.1029/2005JD006568, 2006.

880

881 Fiedler, V., Dal Maso, M., Boy, M., Aufmhoff, H., Hoffmann, J., Schuck, T., Birmili, W., Hanke, M.,

882 Uecker, J., Arnold, F., and Kulmala, M.: The contribution of sulphuric acid to atmospheric particle

883 formation and growth: a comparison between boundary layers in Northern and Central Europe, Atmos.

884 Chem. Phys., 5, 1773–1785, doi: 10.5194/acp-5-1773-2005, 2005.

885

886 Forester, C. D., and Wells, J. R.: Hydroxyl radical yields from reactions of terpene mixtures with ozone,

887 Indoor Air, 21, 400–409, doi: 10.1111/j.1600-0668.2011.00718.x, 2011.

888

889 Freshour, N. A., Carlson, K. K., Melka, Y. A., Hinz, S., Panta, B., and Hanson, D. R.: Amine permeation

890 sources characterized with acid neutralization and sensitivities of an amine mass spectrometer, Atmos.

891 Meas. Tech., 7, 3611–3621, doi: 10.5194/amt-7-3611-2014, 2014.

892

893 Ge, X., Wexler, A. S., and Clegg, S. L.: Atmospheric amines – Part I. A review, Atmos. Env., 45, 524–

894 546, doi: 10.1016/j.atmosenv.2010.10.012, 2011.

895

896 Geron, C., Rasmussen, R., Arnts, R. R., and Guenther, A.: A review and synthesis of monoterpene

897 speciation from forests in the United States, Atmos. Env., 34, 1761–1781, doi: 10.1016/S1352-

898 2310(99)00364-7, 2000.

899

900 Glasoe, W. A., Volz, K., Panta, B., Freshour, N., Bachman, R., Hanson, D. R., McMurry, P. H., and Jen,

901 C.: Sulfuric acid nucleation: An experimental study of the effect of seven bases, J. Geophys. Res.

902 Atmos., 120, 1933–1950, doi: 10.1002/2014JD022730, 2015.

903

904 Hamed, A., Korhonen, H., Sihto, S.-L., Joutsensaari, J., Järvinen, H., Petäjä, T., Arnold, F., Nieminen,

905 T., Kulmala, M., Smith, J. N., Lehtinen, K. E. J., and Laaksonen, A.: The role of relative humidity in

906 continental new particle formation, J. Geophys. Res., 116, D03202, doi: 10.1029/2010JD014186, 2011.

907

908 Hanson, D. R., and Eisele, F. L.: Measurement of prenucleation molecular clusters in the NH_3, H_2SO_4,

909 H_2O system, J. Geophys. Res., 107, D12, 4158, doi: 10.1029/2001JD001100, 2002.

910

911 Hanson, D. R., and Lovejoy, E. R.: Measurement of the thermodynamics of the hydrated dimer and

912 trimer of sulfuric acid, J. Phys. Chem. A, 110, 9525–9528, doi: 10.1021/jp062844w, 2006.

913

914 Hanson, D. R., McMurry, P. H., Jiang, J., Tanner, D., and Huey, L. G.: Ambient pressure proton transfer

915 mass spectrometry: detection of amines and ammonia, Environ. Sci. Technol., 45, 8881–8888, doi:

916 10.1021/es201819a, 2011.

917

918 Hellén, H., Kieloaho, A.-J., and Hakola, H.: Gas-phase alkyl amines in urban air; comparison with a

919 boreal forest site and importance for local atmospheric chemistry, Atmos. Env., 94, 192–197, doi:

920 10.1016/j.atmosenv.2014.05.029, 2014.

921

922 Hirsikko, A., Laakso, L., Hõrrak, U., Aalto, P. P., Kerminen, V.-M., and Kulmala, M.: Annual and size

923 dependent variation of growth rates and ion concentrations in boreal forest, Boreal Env. Res., 10, 357–

924 369, 2005.

925

926 Heinritzi, M., Simon, M., Steiner, G., Wagner, A. C., Kürten, A., Hansel, A., and Curtius, J.:

927 Characterization of the mass-dependent transmission efficiency of a CIMS, Atmos. Meas. Tech., 9,

928 1449–1460, doi: 10.5194/amt-9-1449-2016, 2016.

929

930 Janson, R., and de Serves, C.: Acetone and monoterpene emissions from the boreal forest in northern

931 Europe, Atmos. Env., 35, 4629–4637, doi: 10.1016/S1352-2310(01)00160-1, 2001.

932

933 Jen, C., McMurry, P. H., and Hanson, D. R.: Stabilization of sulfuric acid dimers by ammonia,

934 methylamine, dimethylamine, and trimethylamine, J. Geophys. Res. Atmos., 119, 7502–7514, doi:

935 10.1002/2014JD021592, 2014.

936

937 Jen, C. N., Bachman, R., Zhao, J., McMurry, P. H., and Hanson, D. R.: Diamine-sulfuric acid reactions

938 are a potent source of new particle formation, Geophys. Res. Lett., 43, 867–873, doi:

939 10.1002/2015GL066958, 2016a.

940

941 Jen, C. N., Zhao, J., McMurry, P. H., and Hanson, D. R.: Chemical ionization of clusters formed from

942 sulfuric acid and dimethylamine or diamines, Atmos. Chem. Phys. Discuss., doi:10.5194/acp-2016-492,

943 2016b.

944

945   Jiang, J., Zhao, J., Chen, M., Eisele, F. L., Scheckman, J., Williams, B. J., Kuang, C., and McMurry, P.
946   H.: First measurements of neutral atmospheric cluster and 1-2 nm particle number size distributions
947   during nucleation events, Aerosol Sci. Technol., 45, ii–v, doi: 10.1080/02786826.2010.546817, 2011.
948

949   Jokinen, T., Sipilä, M., Junninen, H., Ehn, M., Lönn, G., Hakala, J., Petäjä, T., Mauldin III, R. L.,
950   Kulmala, M., and Worsnop, D. R.: Atmospheric sulphuric acid and neutral cluster measurements using
951   CI-APi-TOF, Atmos. Chem. Phys., 12, 4117–4125, doi: 10.5194/acp-12-4117-2012, 2012.
952

953   Jokinen, T., Sipilä, M., Richters, S., Kerminen, V.-M., Paasonen, P., Stratmann, F., Worsnop, D.,
954   Kulmala, M., Ehn, M., Herrmann, H., and Berndt, T.: Rapid autooxidation forms highly oxidized RO_2
955   radicals in the atmosphere, Angew. Chem. Int. Ed., 53, 14596–14600, doi: 10.1002/anie.201408566,
956   2014.
957

958   Jokinen, T., Berndt, T., Makkonen, R., Kerminen, V.-M., Junninen, H., Paasonen, P., Stratmann, F.,
959   Herrmann, H., Guenther, A. B., Worsnop, D. R., Kulmala, M., Ehn, M., and Sipilä, M.: Production of
960   extremely low volatile organic compounds from biogenic emissions: Measured yields and atmospheric
961   implications, P. Natl. Acad. Sci. USA, 112, 7123–7128, doi: 10.1073/pnas.1423977112, 2015.
962

963   Junninen, H., Ehn, M., Petäjä, T., Luosujärvi, L., Kotiaho, T., Kostiainen, R., Rohner, U., Gonin, M.,
964   Fuhrer, K., Kulmala, M., and Worsnop, D. R.: A high-resolution mass spectrometer to measure
965   atmospheric ion composition, Atmos. Meas. Tech., 3, 1039–1053, doi: 10.5194/amt-3-1039-2010, 2010.
966

967   Kirkby, J., Curtius, J., Almeida, J., Dunne, E., Duplissy, J., Ehrhart, S., Franchin, A., Gagné, S., Ickes,
968   L., Kürten, A., Kupc, A., Metzger, A., Riccobono, F., Rondo, L., Schobesberger, S., Tsagkogeorgas, G.,
969   Wimmer, D., Amorim, A., Bianchi, F., Breitenlechner, M., David, A., Dommen, J., Downard, A., Ehn,
970   M., Flagan, R.C., Haider, S., Hansel, A., Hauser, D., Jud, W., Junninen, H., Kreissl, F., Kvashin, A.,
971   Laaksonen, A., Lehtipalo, K., Lima, J., Lovejoy, E. R., Makhmutov, V., Mathot, S., Mikkilä, J.,
972   Minginette, P., Mogo, S., Nieminen, T., Onnela, A., Pereira, P., Petäjä, T., Schnitzhofer, R., Seinfeld, J.
973   H., Sipilä, M., Stozhkov, Y., Stratmann, F., Tomé, A., Vanhanen, J., Viisanen, Y., Vrtala, A., Wagner,
974   P. E., Walther, H., Weingartner, E., Wex, H., Winkler, P. M., Carslaw, K. S., Worsnop, D. R.,
975   Baltensperger, U., and Kulmala, M.: Role of sulphuric acid, ammonia and galactic cosmic rays in
976   atmospheric aerosol nucleation, Nature, 476, 429–435, doi: 10.1038/nature10343, 2011.
977

978   Kirkby, J., Duplissy, J., Sengupta, K., Frege, C., Gordon, H., Williamson, C., Heinritzi, M., Simon, M.,
979   Yan, C., Almeida, J., Tröstl, J., Nieminen, T., Ortega, I. K., Wagner, R., Adamov, A., Amorim, A.,
980   Bernhammer, A.-K., Bianchi, F., Breitenlechner, M., Brilke, S., Chen, X., Craven, J., Dias, A., Ehrhart,
981   S., Flagan, R. C., Franchin, A., Fuchs, C., Guida, R., Hakala, J., Hoyle, C. R., Jokinen, T., Junninen, H.,

982   Kangasluoma, J., Kim, J., Krapf, M., Kürten, A., Laaksonen, A., Lehtipalo, K., Makhmutov, V., Mathot,
983   S., Molteni, U., Onnela, A., Peräkylä, O., Piel, F., Petäjä, T., Praplan, A. P., Pringle, K., Rap, A.,
984   Richards, N. A. D., Riipinen, I., Rissanen, M. P., Rondo, L., Sarnela, N., Schobesberger, S., Scott, C.
985   E., Seinfeld, J. H., Sipilä, M., Steiner, G., Stozhkov, Y., Stratmann, F., Tomé, A., Virtanen, A., Vogel,
986   A. L., Wagner, A., Wagner, P. E., Weingartner, E., Wimmer, D., Winkler, P. M., Ye, P., Zhang, X.,
987   Hansel, A., Dommen, J., Donahue, N. M., Worsnop, D. R., Baltensperger, U., Kulmala, M., Carslaw,
988   K. S., and Curtius, J.: Ion-induced nucleation of pure biogenic particles, Nature, 533, 521–526, doi:
989   10.1038/nature17953, 2016.

991   Kuang, C., McMurry, P. H., McCormick, A. V., and Eisele, F. L.: Dependence of nucleation rates on
992   sulfuric acid vapor concentration in diverse atmospheric locations, J. Geophys. Res., 113, D10209, doi:
993   10.1029/2007JD009253, 2008.

995   Kulmala, M., Vehkamäki, H., Petäjä, T., Dal Maso, M., Lauri, A., Kerminen, V.-M., Birmili, W., and
996   McMurry, P. H.: Formation and growth rates of ultrafine atmospheric particles: a review of observations,
997   J. Aerosol Sci., 35, 143–176, doi: 10.1016/j.jaerosci.2003.10.003, 2004.

999   Kulmala, M., Petäjä, T., Nieminen, T,, Sipilä, M., Manninen, H. E., Lehtipalo, K., Dal Maso, M., Aalto,
1000 P. P., Junninen, H., Paasonen, P., Riipinen, I., Lehtinen, K. E. J., Laaksonen, A., and Kerminen, V.-M.:
1001 Measurement of the nucleation of atmospheric aerosol particles, Nature Prot., 7, 1651–1667, doi:
1002 10.1038/nprot.2012.091, 2012.

1004 Kulmala, M., Kontkanen, J., Junninen, H., Lehtipalo, K., Manninen, H. E., Nieminen, T., Petäjä, T.,
1005 Sipilä, M., Schobesberger, S., Rantala, P., Franchin, A., Jokinen, T., Järvinen, E., Äijälä, M.,
1006 Kangasluoma, J., Hakala, J., Aalto, P. P., Paasonen, P., Mikkilä, J., Vanhanen, J., Aalto, J., Hakola, H.,
1007 Makkonen, U., Ruuskanen, T., Mauldin III, R. L., Duplissy, J., Vehkamäki, H., Bäck, J., Kortelainen,
1008 A., Riipinen, I., Kurtén, T., Johnston, M. V., Smith, J. N., Ehn, M., Mentel, T. F., Lehtinen, K. E. J.,
1009 Laaksonen, A., Kerminen, V.-M., and Worsnop, D. R.: Direct observations of atmospheric aerosol
1010 nucleation, Science, 339, 943–946, doi: 10.1126/science.1227385, 2013.

1012 Kürten, A., Rondo, L., Ehrhart, S., and Curtius, J.: Performance of a corona ion source for measurement
1013 of sulfuric acid by chemical ionization mass spectrometry, Atmos. Meas. Technol., 4, 437–443, doi:
1014 10.5194/amt-4-437-2011, 2011.

1016 Kürten, A., Rondo, L., Ehrhart, S., and Curtius, J.: Calibration of a chemical ionization mass
1017 spectrometer for the measurement of gaseous sulfuric acid, J. Phys. Chem. A, 116, 6375–6386, doi:
1018 10.1021/jp212123n, 2012.

1019

1020   Kürten, A., Jokinen, T., Simon, M., Sipilä, M., Sarnela, N., Junninen, H., Adamov, A., Almeida, J.,
1021   Amorim, A., Bianchi, F., Breitenlechner, M., Dommen, J., Donahue, N. M., Duplissy, J., Ehrhart, S.,
1022   Flagan, R. C., Franchin, A., Hakala, J., Hansel, A., Heinritzi, M., Hutterli, M., Kangasluoma, J., Kirkby,
1023   J., Laaksonen, A., Lehtipalo, K., Leiminger, M., Makhmutov, V., Mathot, S., Onnela, A., Petäjä, T.,
1024   Praplan, A. P., Riccobono, F., Rissanen, M. P., Rondo, L., Schobesberger, S., Seinfeld, J. H., Steiner,
1025   G., Tomé, A., Tröstl, J., Winkler, P. M., Williamson, C., Wimmer, D., Ye, P., Baltensperger, U.,
1026   Carslaw, K. S., Kulmala, M., Worsnop, D. R., and Curtius, J.: Neutral molecular cluster formation of
1027   sulfuric acid-dimethylamine observed in real-time under atmospheric conditions, P. Natl. Acad. Sci.
1028   USA, 111, 15019–15024, doi: 10.1073/pnas.1404853111, 2014.

1029

1030   Kürten, A., Münch, S., Rondo, L., Bianchi, F., Duplissy, J., Jokinen, T., Junninen, H., Sarnela, N.,
1031   Schobesberger, S., Simon, M., Sipilä, M., Almeida, J., Amorim, A., Dommen, J., Donahue, N. M.,
1032   Dunne, E. M., Flagan, R. C., Franchin, A., Kirkby, J., Kupc, A., Makhmutov, V., Petäjä, T., Praplan, A.
1033   P., Riccobono, F., Steiner, G., Tomé, A., Tsagkogeorgas, G., Wagner, P. E., Wimmer, D., Baltensperger,
1034   U., Kulmala, M., Worsnop, D. R., and Curtius, J.: Thermodynamics of the formation of sulfuric acid
1035   dimers in the binary (H_2SO_4–H_2O) and ternary (H_2SO_4–H_2O–NH_3) system, Atmos. Chem. Phys., 15,
1036   10701–10721, doi: 10.5194/acp-15-10701-2015, 2015.

1037

1038   Kürten, A., Bianchi, F., Almeida, J., Kupiainen-Määttä, O., Dunne, E. M., Duplissy, J., Williamson, C.,
1039   Barmet, P., Breitenlechner, M., Dommen, J., Donahue, N. M., Flagan, R. C., Franchin, A., Gordon, H.,
1040   Hakala, J., Hansel, A., Heinritzi, M., Ickes, L., Jokinen, T., Kangasluoma, J., Kim, J., Kirkby, J., Kupc,
1041   A., Lehtipalo, K., Leiminger, M., Makhmutov, V., Onnela, A., Ortega, I. K., Petäjä, T., Praplan, A. P.,
1042   Riccobono, F., Rissanen, M. P., Rondo, L., Schnitzhofer, R., Schobesberger, S., Smith, J. N., Steiner,
1043   G., Stozhkov, Y., Tomé, A., Tröstl, J., Tsagkogeorgas, G., Wagner, P. E., Wimmer, D., Ye, P.,
1044   Baltensperger, U., Carslaw, K., Kulmala, M., and Curtius, J.: Experimental particle formation rates
1045   spanning tropospheric sulfuric acid and ammonia abundances, ion production rates and temperatures, J.
1046   Geophys. Res. Atmos., accepted, doi: 10.1002/2015JD023908, 2016.

1047

1048   Kurtén, T., Loukonen, V., Vehkamäki, H., and Kulmala, M.: Amines are likely to enhance neutral and
1049   ion-induced sulfuric acid-water nucleation in the atmosphere more effectively than ammonia, Atmos.
1050   Chem. Phys., 8, 4095–4103, doi: 10.5194/acp-8-4095-2008, 2008.

1051

1052   Lehtinen, K. E. J., Dal Maso, M., Kulmala, M., and Kerminen, V.-M.: Estimating nucleation rates from
1053   apparent particle formation rates and vice versa: Revised formulation of the Kerminen–Kulmala
1054   equation, J. Aerosol Sci., 38, 988–994, doi: 10.1016/j.jaerosci.2007.06.009, 2007.

1055

1056 Lehtipalo, K., Rondo, L., Kontkanen, J., Schobesberger, S., Jokinen, T., Sarnela, N., Kürten, A., Ehrhart,
1057 S., Franchin, A., Nieminen, T., Riccobono, F., Sipilä, M., Yli-Juuti, T., Duplissy, J., Adamov, A., Ahlm,
1058 L., Almeida, J., Amorim, A., Bianchi, F., Breitenlechner, M., Dommen, J., Downard, A. J., Dunne, E.
1059 M., Flagan, R. C., Guida, R., Hakala, J., Hansel, A., Jud, W., Kangasluoma, J., Kerminen, V.-M.,
1060 Keskinen, H., Kim, J., Kirkby, J., Kupc, A., Kupiainen-Määttä, O., Laaksonen, A., Lawler, M. J.,
1061 Leiminger, M., Mathot, S., Olenius, T., Ortega, I. K., Onnela, A., Petäjä, T., Praplan, A., Rissanen, M.
1062 P., Ruuskanen, T., Santos, F. D., Schallhart, S., Schnitzhofer, R., Simon, M., Smith, J. N., Tröstl, J.,
1063 Tsagkogeorgas, G., Tomé, A., Vaattovaara, P., Vehkamäki, H., Vrtala, A. E., Wagner, P. E.,
1064 Williamson, C., Wimmer, D., Winkler, P. M., Virtanen, A., Donahue, N. M., Carslaw, K. S.,
1065 Baltensperger, U., Riipinen, I., Curtius, J., Worsnop D. R., and Kulmala, M.: The effect of acid-base
1066 clustering and ions on the growth of atmospheric nano-particles, Nat. Commun., 7, 11594, doi:
1067 10.1038/ncomms11594, 2016.

1069 Luts, A., Parts, T.-E., Hõrrak, U., Junninen, H., and Kulmala, M.: Composition of negative air ions as a
1070 function of ion age and selected trace gases: Mass- and mobility distribution, J. Aerosol Sci., 42 820–
1071 838, doi: 10.1016/j.jaerosci.2011.07.007, 2011.

1073 Mauldin III, R. L., Berndt, T., Sipilä, M., Paasonen, P., Petäjä, T., Kim, S., Kurtén, T., Stratmann, F.,
1074 Kerminen, V.-M., and Kulmala, M.: A new atmospherically relevant oxidant of sulphur dioxide, Nature,
1075 488, 193–196, doi: 10.1038/nature11278, 2012.

1077 Mauldin III, R. L., Rissanen, M. P., Petäjä, T., and Kulmala, M.: Furthering information from OH and
1078 $HO_2 + RO_2$ observations using a high resolution time of flight mass spectrometer, Atmos. Meas. Tech.
1079 Discuss., doi: 10.5194/amt-2015-398, 2016.

1081 Merikanto, J., Spracklen, D. V., Mann, G. W., Pickering, S. J., and Carslaw, K. S.: Impact of nucleation
1082 on global CCN, Atmos. Chem. Phys., 9, 8601–8616, doi: 10.5194/acp-9-8601-2009, 2009.

1084 Metzger, A., Verheggen, B., Dommen, J., Duplissy, J., Prevot, A. S. H., Weingartner, E., Riipinen, I.,
1085 Kulmala, M., Spracklen, D. V., Carslaw, K. S., and Baltensperger, U.: Evidence for the role of organics
1086 in aerosol particle formation under atmospheric conditions, P. Natl. Acad. Sci. USA, 107, 6646–6651,
1087 doi: 10.1073/pnas.0911330107, 2010.

1089 Mikkonen, S., Romakkaniemi, S., Smith, J. N., Korhonen, H., Petäjä, T., Plass-Duelmer, C., Boy, M.,
1090 McMurry, P. H., Lehtinen, K. E. J., Joutsensaari, J., Hamed, A., Mauldin III, R. L., Birmili, W., Spindler,
1091 G., Arnold, F., Kulmala, M., and Laaksonen, A.: A statistical proxy for sulphuric acid concentration,
1092 Atmos. Chem. Phys., 11, 11319–11334, doi: 10.5194/acp-11-11319-2011, 2011.

1093

1094 Monks, P. S.: Gas-phase radical chemistry in the troposphere, Chem. Soc. Rev., 34, 376–395, doi:
1095 10.1039/B307982C, 2005.

1096

1097 Mutzel, A., Poulain, L., Berndt, T., Iinuma, Y., Rodigast, M., Böge, O., Richters, S., Spindler, G., Sipilä,
1098 M., Jokinen, T., Kulmala, M., and Herrmann, H.: Highly oxidized multifunctional organic compounds
1099 observed in tropospheric particles: A field and laboratory study, Environ. Sci. Technol., 49, 7754–7761,
1100 doi: 10.1021/acs.est.5b00885, 2015.

1101

1102 Nel, A.: Air pollution–related illness: Effects of particles, Science, 308, 804–806, doi:
1103 10.1126/science.1108752, 2005.

1104

1105 Nielsen, C. J., Herrmann, H., and Weller, C.: Atmospheric chemistry and environmental impact of the
1106 use of amines in carbon capture and storage (CCS), Chem. Soc. Rev., 41, 6684–6704, doi:
1107 10.1039/c2cs35059a, 2012.

1108 Nieminen, T., Yli-Juuti, T., Manninen, H. E., Petäjä, T., Kerminen, V.-M., and Kulmala, M.: Technical
1109 note: New particle formation event forecasts during PEGASOS–Zeppelin Northern mission 2013 in
1110 Hyytiälä, Finland, Atmos. Chem. Phys., 15, 12385–12396, doi: 10.5194/acp-15-12385-2015, 2015.

1111

1112 Ortega, I. K., Kupiainen, O., Kurtén, T., Olenius, T., Wilkman, O., McGrath, M. J., Loukonen, V., and
1113 Vehkamäki, H.: From quantum chemical formation free energies to evaporation rates, Atmos. Chem.
1114 Phys., 12, 225–235, doi: 10.5194/acp-12-225-2012, 2012.

1115

1116 Ortega, I. K., Olenius, T., Kupiainen-Määttä, O., Loukonen, V., Kurtén, T., and Vehkamäki, H.:
1117 Electrical charging changes the composition of sulfuric acid–ammonia/dimethylamine clusters, Atmos.
1118 Chem. Phys., 14, 7995–8007, doi: 10.5194/acp-14-7995-2014, 2014.

1119

1120 Paasonen, P., Nieminen, T., Asmi, E., Manninen, H. E., Petäjä, T., Plass-Dülmer, C., Flentje, H., Birmili,
1121 W., Wiedensohler, A., Hõrrak, U., Metzger, A., Hamed, A., Laaksonen, A., Facchini, M. C., Kerminen,
1122 V.-M., and Kulmala, M.: On the roles of sulphuric acid and low-volatility organic vapours in the initial
1123 steps of atmospheric new particle formation, Atmos. Chem. Phys., 10, 11223–11242, doi: 10.5194/acp-
1124 10-11223-2010, 2010.

1125

1126 Petäjä, T., Mauldin, III, R. L., Kosciuch, E., McGrath, J., Nieminen, T., Paasonen, P., Boy, M., Adamov,
1127 A., Kotiaho, T., and Kulmala, M.: Sulfuric acid and OH concentrations in a boreal forest site, Atmos.
1128 Chem. Phys., 9, 7435–7448, doi: 10.5194/acp-9-7435-2009, 2009.

1129

1130 Plane, J. M. C., Joseph, D. M., Allan, B. J., Ashworth, S. H., and Francisco, J. S.: An experimental and
1131 theoretical study of the reactions OIO + NO and OIO + OH, J. Phys. Chem. A, 110, 93–100, doi:
1132 10.1021/jp055364y, 2006.

1133

1134 Praplan, A. P., Schobesberger, S., Bianchi, F., Rissanen, M. P., Ehn, M., Jokinen, T., Junninen, H.,
1135 Adamov, A., Amorim, A., Dommen, J., Duplissy, J., Hakala, J., Hansel, A., Heinritzi, M., Kangasluoma,
1136 J., Kirkby, J., Krapf, M., Kürten, A., Lehtipalo, K., Riccobono, F., Rondo, L., Sarnela, N., Simon, M.,
1137 Tomé, A., Tröstl, J., Winkler, P. M., Williamson, C., Ye, P., Curtius, J., Baltensperger, U., Donahue, N.
1138 M., Kulmala, M., and Worsnop, D. R.: Elemental composition and clustering behaviour of α-pinene
1139 oxidation products for different oxidation conditions, Atmos. Chem. Phys., 15, 4145–4159, doi:
1140 10.5194/acp-15-4145-2015, 2015.

1141

1142 Rantala, P., Taipale, R., Aalto, J., Kajos, M. K., Patokoski, J., Ruuskanen, T. M., and Rinne, J.:
1143 Continuous flux measurements of VOCs using PTR-MS – reliability and feasibility of disjunct-eddy-
1144 covariance, surface-layer-gradient, and surface-layer-profile methods, Boreal Env. Res., 19 (suppl. B),
1145 87–107, 2014.

1146

1147 Rohrer, F., and Berreheim, H.: Strong correlation between levels of tropospheric hydroxyl radicals and
1148 solar ultraviolet radiation, Nature, 442, 184–187, doi: 10.1038/nature04924, 2006.

1149

1150 Riccobono, F., Schobesberger, S., Scott, C. E., Dommen, J., Ortega, I. K., Rondo, L., Almeida, J.,
1151 Amorim, A., Bianchi, F., Breitenlechner, M., David, A., Downard, A., Dunne, E. M., Duplissy, J.,
1152 Ehrhart, S., Flagan, R. C., Franchin, A., Hansel, A., Junninen, H., Kajos, M., Keskinen, H., Kupc, A.,
1153 Kürten, A., Kvashin, A. N., Laaksonen, A., Lehtipalo, K., Makhmutov, V., Mathot, S., Nieminen, T.,
1154 Onnela, A., Petäjä, T., Praplan, A. P., Santos, F. D., Schallhart, S., Seinfeld, J. H., Sipilä, M., Spracklen,
1155 D. V., Stozhkov, Y., Stratmann, F., Tomé, A., Tsagkogeorgas, G., Vaattovaara, P., Viisanen, Y., Vrtala,
1156 A., Wagner, P. E., Weingartner, E., Wex, H., Wimmer, D., Carslaw, K. S., Curtius, J., Donahue, N. M.,
1157 Kirkby, J., Kulmala, M., Worsnop, D. R., and Baltensperger, U.: Oxidation products of biogenic
1158 emissions contribute to nucleation of atmospheric particles, Science, 344, 717–721, doi:
1159 10.1126/science.1243527, 2014.

1160

1161 Rondo, L., Kürten, A., Ehrhart, S., Schobesberger, S., Franchin, A., Junninen, H., Petäjä, T., Sipilä, M.,
1162 Worsnop, D. R., and Curtius, J.: Effect of ions on the measurement of sulfuric acid in the CLOUD
1163 experiment at CERN, Atmos. Meas. Tech., 7, 3849–3859, doi: 10.5194/amt-7-3849-2014, 2014.

1164

1165   Saiz-Lopez, A., Plane, J. M. C., Baker, A. R., Carpenter, L. J., von Glasow, R., Martín, J. C. G.,

1166   McFiggans, G., and Saunders, R. W.: Atmospheric chemistry of iodine, Chem. Rev., 112, 1773–1804,

1167   doi: 10.1021/cr200029u, 2012.

1168

1169   Saiz-Lopez, A., Baidar, S., Cuevas, C. A., Koenig, T. K., Fernandez, R. P., Dix, B., Kinnison, D. E.,

1170   Lamarque, J.-F. , Rodriguez-Lloveras, X., Campos, T. L., and Volkamer, R.: Injection of iodine to the

1171   stratosphere, Geophys. Res. Lett., 42, 6852–6859, doi: 10.1002/2015GL064796, 2015.

1172

1173   Sarnela, N., Jokinen, T., Nieminen, T., Lehtipalo, K., Junninen, H., Kangasluoma, J., Hakala, J., Taipale,

1174   R., Schobesberger, S., Sipilä, M., Larnimaa, K., Westerholm, H., Heijari, J., Kerminen, V.-M., Petäjä,

1175   T., and Kulmala, M.: Sulphuric acid and aerosol particle production in the vicinity of an oil refinery,

1176   Atmos. Env., 119, 156–166, doi: 10.1016/j.atmosenv.2015.08.033, 2015.

1177

1178   Sarwar, G., Fahey, K., Kwok, R., Gilliam, R. C., Roselle, S. J., Mathur, R., Xue, J., Yu, J., and Carter,

1179   W. P. L.: Potential impacts of two SO_2 oxidation pathways on regional sulphate concentrations:

1180   Aqueous-phase oxidation by NO_2 and gas-phase oxidation by stabilized Criegee intermediate, Atmos.

1181   Env., 68, 186–197, doi: 10.1016/j.atmosenv.2012.11.036, 2013.

1182

1183   Schade, G. W., and Crutzen, P. J.: Emission of aliphatic amines from animal husbandry and their

1184   reactions: Potential source of N_2O and HCN, J. Atmos. Chem., 22, 319–346, doi: 10.1007/BF00696641,

1185   1995.

1186

1187   Schobesberger, S., Junninen, H., Bianchi, F., Lönn, G., Ehn, M., Lehtipalo, K., Dommen, J., Ehrhart,

1188   S., Ortega, I. K., Franchin, A., Nieminen, T., Riccobono, F., Hutterli, M., Duplissy, J., Almeida, J.,

1189   Amorim, A., Breitenlechner, M., Downard, A. J., Dunne, E. M., Flagan, R. C., Kajos, M., Keskinen, H.,

1190   Kirkby, J., Kupc, A., Kürten, A., Kurtén, T., Laaksonen, A., Mathot, S., Onnela, A., Praplan, A. P.,

1191   Rondo, L., Santos, F. D., Schallhart, S., Schnitzhofer, R., Sipilä, M., Tomé, A., Tsagkogeorgas, G.,

1192   Vehkamäki, H., Wimmer, D., Baltensperger, U., Carslaw, K. S., Curtius, J., Hansel, A., Petäjä, T.,

1193   Kulmala, M., Donahue, N. M., and Worsnop, D. R.: Molecular understanding of atmospheric particle

1194   formation from sulfuric acid and large oxidized organic molecules, Proc. Natl. Acad. Sci. USA, 110,

1195   17223–17228, doi: 10.1073/pnas.1306973110, 2013.

1196

1197   Sihto, S.-L., Kulmala, M., Kerminen, V.-M., Dal Maso, M., Petäjä, T., Riipinen, I., Korhonen, H.,

1198   Arnold, F., Janson, R., Boy, M., Laaksonen, A., and Lehtinen, K. E. J.: Atmospheric sulphuric acid and

1199   aerosol formation: implications from atmospheric measurements for nucleation and early growth

1200   mechanisms, Atmos. Chem. Phys., 6, 4079–4091, doi: 10.5194/acp-6-4079-2006, 2006.

1201

Simon, M., Heinritzi, M., Herzog, S., Leiminger, M., Bianchi, F., Praplan, A., Dommen, J., Curtius, J., and Kürten, A.: Detection of dimethylamine in the low pptv range using nitrate chemical ionization atmospheric pressure interface time-of-flight (CI-APi-TOF) mass spectrometry, Atmos. Meas. Tech., 9, 2135–2145, doi: 10.5194/amt-9-2135-2016, 2016.

Sintermann, J., Schallhart, S., Kajos, M., Jocher, M., Bracher, A., Münger, A., Johnson, D., Neftel, A., and Ruuskanen, T.: Trimethylamine emissions in animal husbandry, Biogeosciences, 11, 5073–5085, doi: 10.5194/bg-11-5073-2014, 2014.

Sipilä, M., Jokinen, T., Berndt, T., Richters, S., Makkonen, R., Donahue, N. M., Mauldin III, R. L., Kurtén, T., Paasonen, P., Sarnela, N., Ehn, M., Junninen, H., Rissanen, M. P., Thornton, J., Stratmann, F., Herrmann, H., Worsnop, D. R., Kulmala, M., Kerminen, V.-M., and Petäjä, T.: Reactivity of stabilized Criegee intermediates (sCIs) from isoprene and monoterpene ozonolysis toward SO_2 and organic acids, Atmos. Chem. Phys., 14, 12143–12153, doi: 10.5194/acp-14-12143-2014, 2014.

Sipilä, M., Sarnela, N., Jokinen, T., Junninen, H., Hakala, J., Rissanen, M. P., Praplan, A., Simon, M., Kürten, A., Bianchi, F., Dommen, J., Curtius, J., Petäjä, T., and Worsnop, D. R.: Bisulfate – cluster based atmospheric pressure chemical ionization mass spectrometer for high-sensitivity (< 100 ppqV) detection of atmospheric dimethyl amine: proof-of-concept and first ambient data from boreal forest, Atmos. Meas. Tech., 8, 4001–4011, doi: 10.5194/amt-8-4001-2015, 2015.

Stein, A. F., Draxler, R. R, Rolph, G. D., Stunder, B. J. B., Cohen, M. D., and Ngan, F.: NOAA's HYSPLIT atmospheric transport and dispersion modeling system, Bull. Amer. Meteor. Soc., 96, 2059–2077, doi: 10.1175/BAMS-D-14-00110.1, 2015.

Tani, A., Hayward, S., and Hewitt, C. N.: Measurement of monoterpenes and related compounds by proton transfer reaction-mass spectrometry (PTR-MS), Int. J. Mass Spectrom., 223, 561–578, doi: 10.1016/S1387-3806(02)00880-1, 2003.

Vanhanen, J. , Mikkilä, J. , Lehtipalo, K. , Sipilä, M. , Manninen, H. E. , Siivola, E. , Petäjä, T., and Kulmala, M.: Particle size magnifier for nano-CN detection, Aerosol Sci. Technol., 45, 533–542, doi: 10.1080/02786826.2010.547889, 2011.

von Bobrutzki, K., Braban, C. F., Famulari, D., Jones, S. K., Blackall, T., Smith, T. E. L., Blom, M., Coe, H., Gallagher, M., Ghalaieny, M., McGillen, M. R., Percival, C. J., Whitehead, J. D., Ellis, R., Murphy, J., Mohacsi, A., Pogany, A., Junninen, H., Rantanen, S., Sutton, M. A., and Nemitz, E.: Field

1238 inter-comparison of eleven atmospheric ammonia measurement techniques, Atmos. Meas. Tech., 3, 91–
1239 112, doi: 10.5194/amt-3-91-2010, 2010.

1240

1241 Weber, R. J., Marti, J. J., McMurry, P. H., Eisele, F. L., Tanner, D. J., and Jefferson, A.: Measurements
1242 of new particle formation and ultrafine particle growth rates at a clean continental site, J. Geophys. Res.,
1243 102, D4, 4375–4385, doi: 10.1029/96JD03656, 1997.

1244

1245 You, Y., Kanawade, V. P., de Gouw, J. A., Guenther, A. B., Madronich, S., Sierra-Hernández, M. R.,
1246 Lawler, M., Smith, J. N., Takahama, S., Ruggeri, G., Koss, A., Olson, K., Baumann, K., Weber, R. J.,
1247 Nenes, A., Guo, H., Edgerton, E. S., Porcelli, L., Brune, W. H., Goldstein, A. H., and Lee, S.-H.:
1248 Atmospheric amines and ammonia measured with a chemical ionization mass spectrometer (CIMS),
1249 Atmos. Chem. Phys., 14, 12181–12194, doi: 10.5194/acp-14-12181-2014, 2014.

1250

1251 Yu, H., and Lee, S.-H.: Chemical ionisation mass spectrometry for the measurement of atmospheric
1252 amines, Env. Chem., 9, 190–201, doi: 10.1071/EN12020, 2012.

1253

1254 Zhang, R., Khalizov, A., Wang, L., Hu, M., and Xu, W.: Nucleation and growth of nanoparticles in the
1255 atmosphere, Chem. Rev., 1957–2011, doi: 10.1021/cr2001756, 2012.

1256

1257 Zhao, J., Eisele, F. L., Titcombe, M., Kuang, C., and McMurry, P. H.: Chemical ionization mass
1258 spectrometric measurements of atmospheric neutral clusters using the cluster-CIMS, J. Geophys. Res.,
1259 115, D08205, doi: 10.1029/2009JD012606, 2010.

1260

1261 Zhao, J., Smith, J. N., Eisele, F. L., Chen, M., Kuang, C., and McMurry, P. H.: Observation of neutral
1262 sulfuric acid-amine containing clusters in laboratory and ambient measurements, Atmos. Chem. Phys.,
1263 11, 10823–10836, doi: 10.5194/acp-11-10823-2011, 2011.

1264

1265 Zhao, J., Ortega, J., Chen, M., McMurry, P. H., and Smith, J. N.: Dependence of particle nucleation and
1266 growth on high-molecular-weight gas-phase products during ozonolysis of α-pinene, Atmos. Chem.
1267 Phys., 13, 7631–7644, doi: 10.5194/acp-13-7631-2013, 2013.

1268 **Table 1.** List of ions used in the identification of sulfuric acid (monomer and dimer), iodic acid,

1269 ammonia, amines (C1, C2, C3, C4 and C6) and dimethylnitrosamine. Cattle farms in the vicinity of the

1270 measurement site are expected to be a source for the listed amines (Ge et al., 2011).

1271

Ion	Exact mass	Neutral compound
HSO_4^-, $(HNO_3)HSO_4^-$	96.9601, 159.9557	sulfuric acid monomer
$(H_2SO_4)HSO_4^-$, $(HNO_3)(H_2SO_4)HSO_4^-$	194.9275, 257.9231	sulfuric acid dimer
IO_3^-, $(H_2O)IO_3^-$, $(HNO_3)IO_3^-$	174.8898, 192.9003, 237.8854	iodic acid
$(NH_3)(HNO_3)_{1,2}NO_3^-$	142.0106, 205.0062	ammonia
$(CH_5N)(HNO_3)_{1,2}NO_3^-$	156.0262, 219.0219	C1-amines (e.g. methylamine)
$(C_2H_7N)(HNO_3)_{1,2}NO_3^-$	170.0419, 233.0375	C2-amines (e.g. ethylamine, dimethylamine)
$(C_3H_9N)(HNO_3)_{1,2}NO_3^-$	184.0575, 247.0532	C3-amines (e.g. trimethylamine, propylamine)
$(C_4H_{11}N)(HNO_3)_{1,2}NO_3^-$	198.0732, 261.0688	C4-amines (e.g. diethylamine, butylamine)
$(C_6H_{15}N)(HNO_3)_{1,2}NO_3^-$	226.1045, 289.1001	C6-amines (e.g. triethylamine)
$(C_2H_6N_2O)(HNO_3)_{1,2}NO_3^-$	199.0320, 262.0277	dimethylnitrosamine

1272

1273 **Table 2.** Peak list of the highly oxidized organic molecules (HOM) used in this study.

1274

| Ion sum formula	Cluster ion	Exact mass	Compound
$C_{10}H_{15}NO_9^-$	$(C_{10}H_{15}O_6)NO_3^-$	293.0752	HOM RO_2 radical
$C_{10}H_{15}NO_{10}^-$	$(C_{10}H_{15}O_7)NO_3^-$	309.0701	HOM RO_2 radical
$C_{10}H_{15}NO_{11}^-$	$(C_{10}H_{15}O_8)NO_3^-$	325.0651	HOM RO_2 radical
$C_{10}H_{15}NO_{12}^-$	$(C_{10}H_{15}O_9)NO_3^-$	341.0600	HOM RO_2 radical
$C_{10}H_{15}NO_{13}^-$	$(C_{10}H_{15}O_{10})NO_3^-$	357.0549	HOM RO_2 radical
$C_{10}H_{15}NO_{15}^-$	$(C_{10}H_{15}O_{12})NO_3^-$	389.0447	HOM RO_2 radical
$C_8H_{12}NO_{11}^-$	$(C_8H_{12}O_8)NO_3^-$	298.0416	HOM monomer
$C_9H_{14}NO_{12}^-$	$(C_9H_{14}O_9)NO_3^-$	328.0521	HOM monomer
$C_{10}H_{14}NO_{10}^-$	$(C_{10}H_{14}O_7)NO_3^-$	308.0623	HOM monomer
$C_{10}H_{14}NO_{11}^-$	$(C_{10}H_{14}O_8)NO_3^-$	324.0572	HOM monomer
$C_{10}H_{14}NO_{12}^-$	$(C_{10}H_{14}O_9)NO_3^-$	340.0521	HOM monomer
$C_{10}H_{14}NO_{13}^-$	$(C_{10}H_{14}O_{10})NO_3^-$	356.0471	HOM monomer
$C_{10}H_{14}NO_{14}^-$	$(C_{10}H_{14}O_{11})NO_3^-$	372.0420	HOM monomer
$C_{10}H_{16}NO_9^-$	$(C_{10}H_{16}O_6)NO_3^-$	294.0831	HOM monomer
$C_{10}H_{16}NO_{10}^-$	$(C_{10}H_{16}O_7)NO_3^-$	310.0780	HOM monomer
$C_{10}H_{16}NO_{11}^-$	$(C_{10}H_{16}O_8)NO_3^-$	326.0729	HOM monomer
$C_{10}H_{16}NO_{12}^-$	$(C_{10}H_{16}O_9)NO_3^-$	342.0678	HOM monomer
$C_{10}H_{16}NO_{13}^-$	$(C_{10}H_{16}O_{10})NO_3^-$	358.0627	HOM monomer
$C_{10}H_{16}NO_{14}^-$	$(C_{10}H_{16}O_{11})NO_3^-$	374.0576	HOM monomer
$C_{10}H_{15}N_2O_{10}^-$	$(C_{10}H_{15}NO_7)NO_3^-$	323.0732	HOM nitrate
$C_{10}H_{15}N_2O_{11}^-$	$(C_{10}H_{15}NO_8)NO_3^-$	339.0681	HOM nitrate
$C_{10}H_{15}N_2O_{12}^-$	$(C_{10}H_{15}NO_9)NO_3^-$	355.0630	HOM nitrate
$C_{10}H_{15}N_2O_{13}^-$	$(C_{10}H_{15}NO_{10})NO_3^-$	371.0580	HOM nitrate
$C_{10}H_{15}N_2O_{14}^-$	$(C_{10}H_{15}NO_{11})NO_3^-$	387.0529	HOM nitrate
$C_{10}H_{15}N_2O_{15}^-$	$(C_{10}H_{15}NO_{12})NO_3^-$	403.0478	HOM nitrate
$C_{10}H_{15}N_2O_{16}^-$	$(C_{10}H_{15}NO_{13})NO_3^-$	419.0427	HOM nitrate
$C_{10}H_{16}N_3O_{11}^-$	$(C_{10}H_{16}N_2O_8)NO_3^-$	354.0790	HOM di-nitrate
$C_{10}H_{17}N_4O_{14}^-$	$(C_{10}H_{16}N_2O_8)(HNO_3)NO_3^-$	417.0747	HOM di-nitrate
$C_{10}H_{16}N_3O_{12}^-$	$(C_{10}H_{16}N_2O_9)NO_3^-$	370.0739	HOM di-nitrate
$C_{10}H_{17}N_4O_{15}^-$	$(C_{10}H_{16}N_2O_9)(HNO_3)NO_3^-$	433.0696	HOM di-nitrate
$C_{10}H_{16}N_3O_{13}^-$	$(C_{10}H_{16}N_2O_{10})NO_3^-$	386.0689	HOM di-nitrate
$C_{10}H_{17}N_4O_{16}^-$	$(C_{10}H_{16}N_2O_{10})(HNO_3)NO_3^-$	449.0645	HOM di-nitrate
$C_{19}H_{30}NO_{16}^-$	$(C_{19}H_{30}O_{13})NO_3^-$	528.1570	HOM dimer
$C_{19}H_{30}NO_{17}^-$	$(C_{19}H_{30}O_{14})NO_3^-$	544.1519	HOM dimer
$C_{20}H_{28}NO_{16}^-$	$(C_{20}H_{28}O_{13})NO_3^-$	538.1414	HOM dimer
$C_{20}H_{28}NO_{17}^-$	$(C_{20}H_{28}O_{14})NO_3^-$	554.1363	HOM dimer
$C_{20}H_{28}NO_{18}^-$	$(C_{20}H_{28}O_{15})NO_3^-$	570.1312	HOM dimer
$C_{20}H_{28}NO_{19}^-$	$(C_{20}H_{28}O_{16})NO_3^-$	586.1261	HOM dimer
$C_{20}H_{28}NO_{20}^-$	$(C_{20}H_{28}O_{17})NO_3^-$	602.1210	HOM dimer
$C_{20}H_{28}NO_{21}^-$	$(C_{20}H_{28}O_{18})NO_3^-$	618.1159	HOM dimer
$C_{20}H_{28}NO_{22}^-$	$(C_{20}H_{28}O_{19})NO_3^-$	634.1108	HOM dimer
$C_{20}H_{28}NO_{23}^-$	$(C_{20}H_{28}O_{20})NO_3^-$	650.1058	HOM dimer
$C_{20}H_{30}NO_{17}^-$	$(C_{20}H_{30}O_{14})NO_3^-$	556.1519	HOM dimer

1275
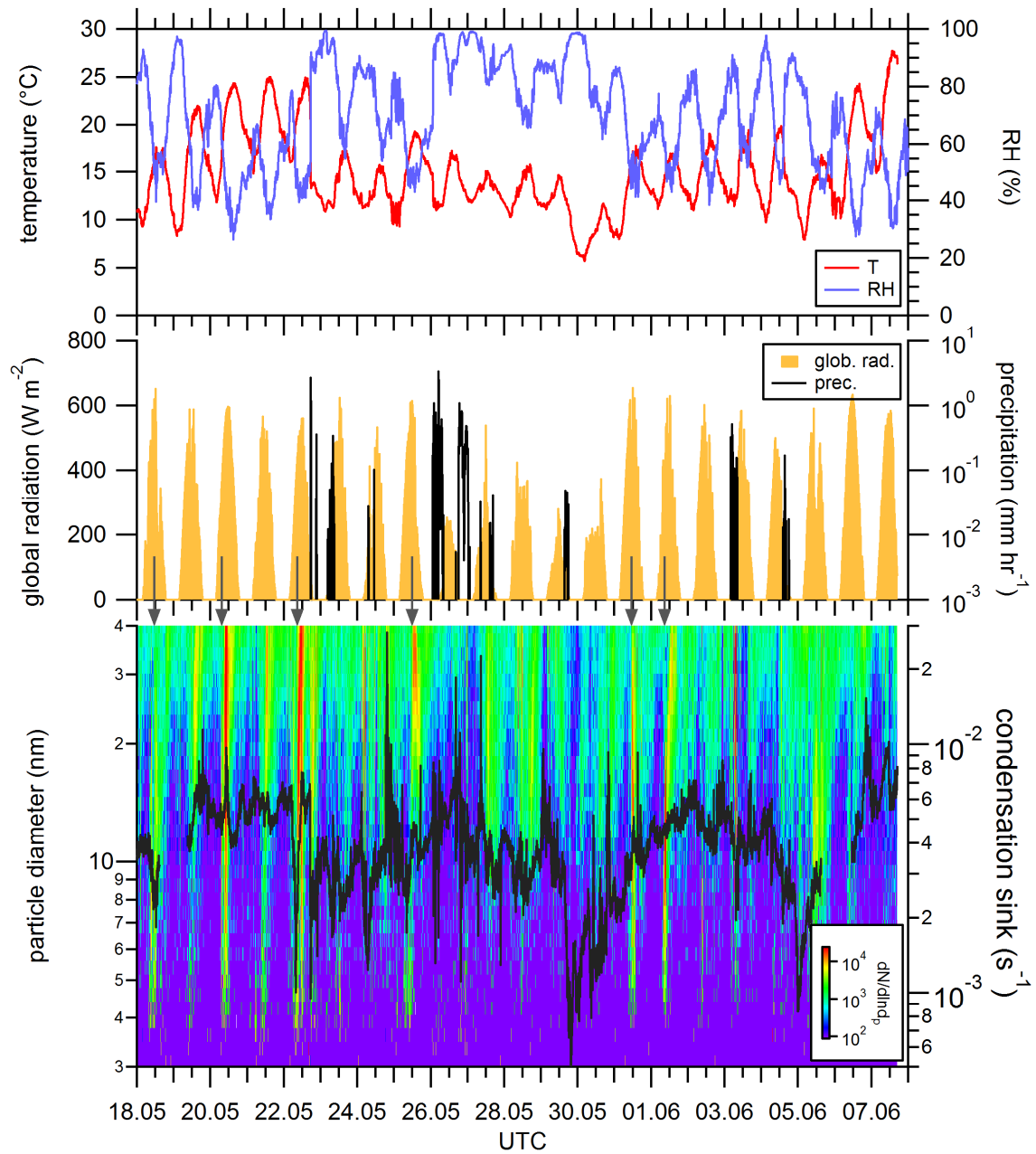
Fig. 1. Overview of the different parameters measured between May 18 and June 8, 2014. Temperature (T) and relative humidity (RH) are shown in the upper panel, the center panel shows the global radiation and precipitation, while the bottom panel shows the number size distribution measured by the nano-DMA together with the condensation sink (black line). Grey arrows above the bottom panel indicate days when significant NPF was observed.

1282
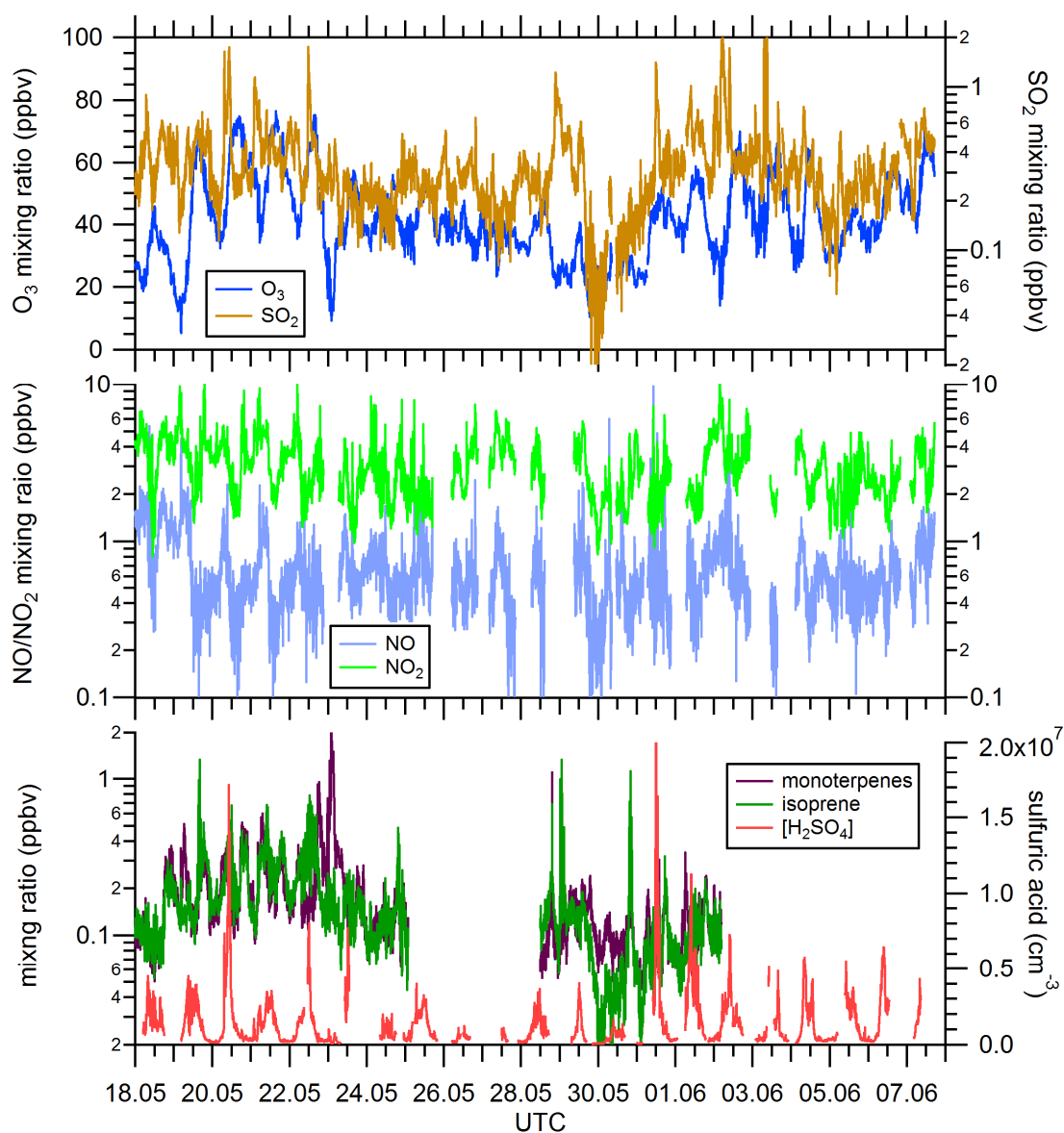
Fig. 2. Overview of the trace gas measurements between May 18 and June 8, 2014. The SO_2 and O_3
mixing ratios are shown in the upper panel, the NO and NO_2 mixing ratios are shown in the center panel
and the bottom panel shows the sulfuric acid monomer concentration ($[H_2SO_4]$) together with the
isoprene and monoterpene mixing ratios.
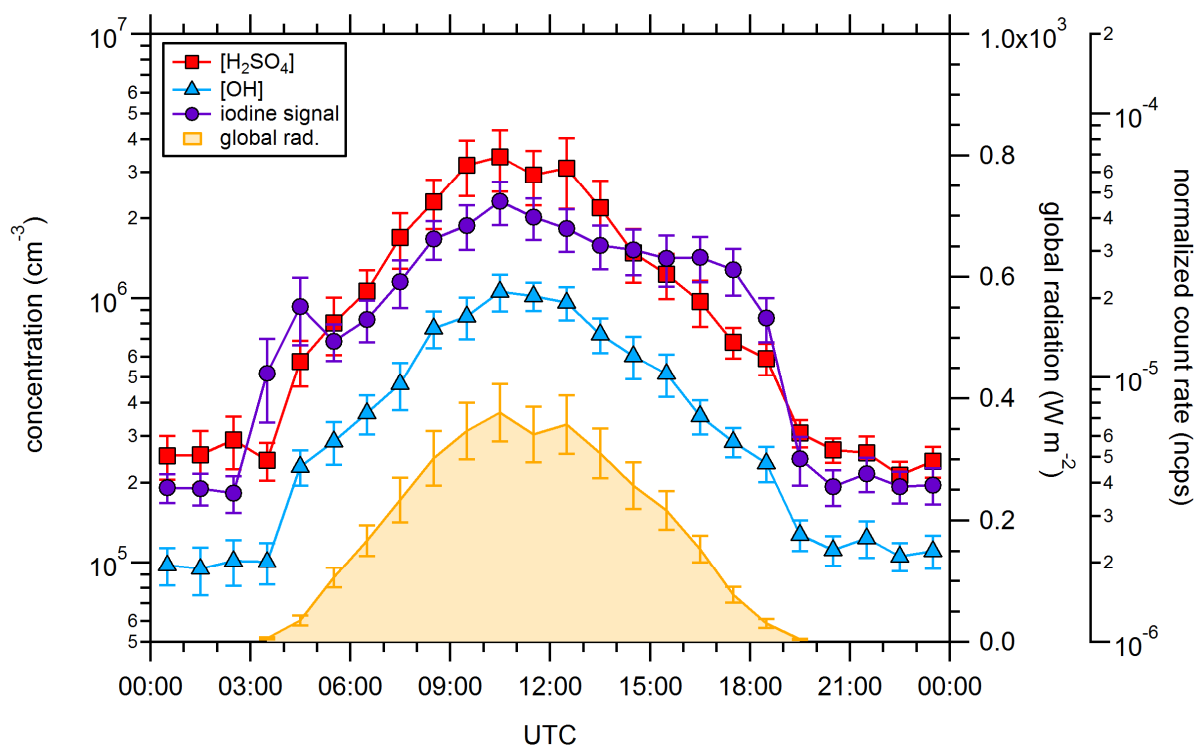
Fig. 3. Diurnal averages for the sulfuric acid ([H$_2$SO$_4$]) and the calculated hydroxyl radical ([OH]) concentrations (axis on the left). The iodine signal is not converted into a concentration, instead the normalized count rates per second (ncps) are shown (axis on the right). A value of 5×10^{-5} ncps for iodine would correspond to a concentration of 3×10^{5} molecule cm^{-3} applying the same conversion factor for iodic acid as for sulfuric acid. The global radiation indicates that all signals are related to photo-chemistry. Error bars indicate one standard deviation for the 30-minute averaged values.
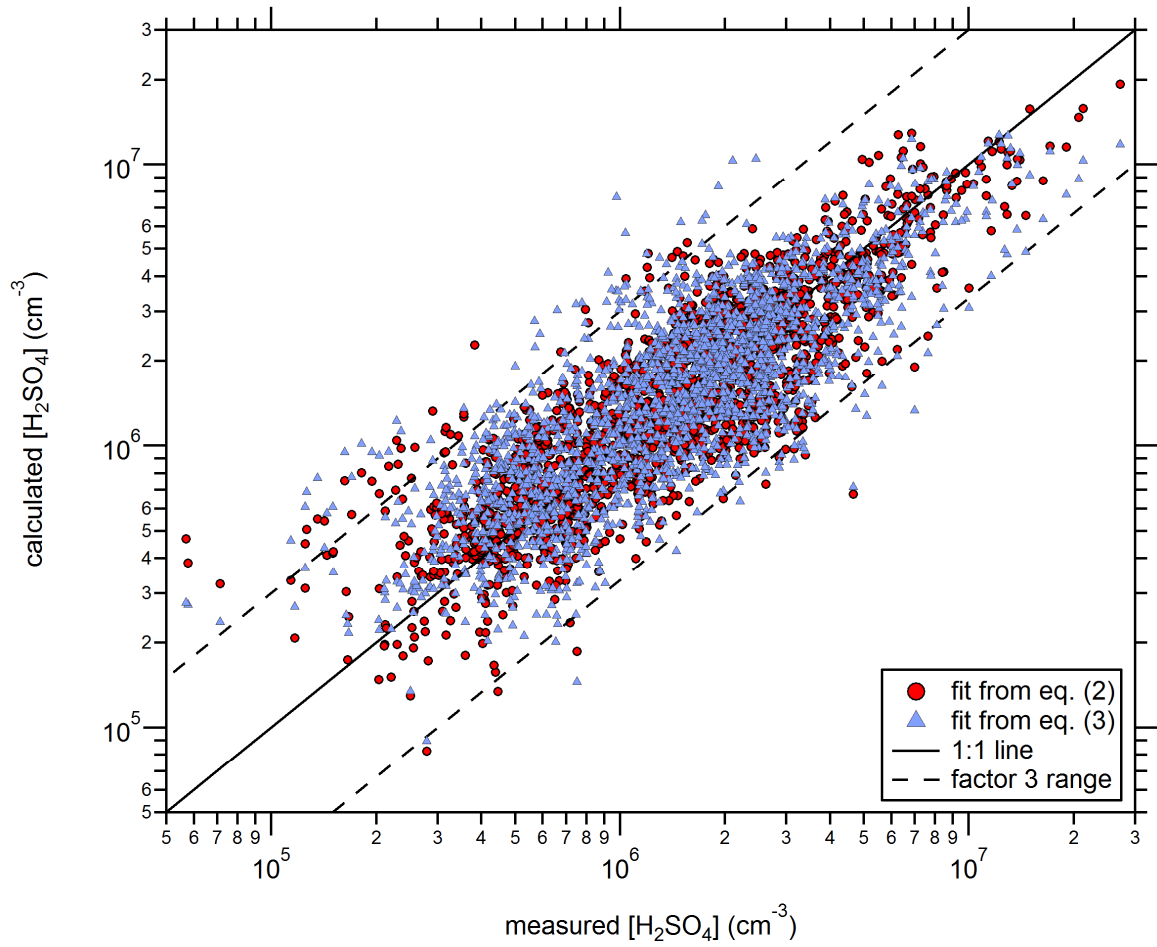
Fig. 4. Calculated [H_2SO_4] as a function of the measured concentrations. Only data points where the global radiation exceeded 50 W m^{-2} were considered in deriving the fit parameters for equations (2) and (3). The red circles take into account SO_2, global radiation (*Rad*), condensation sink (*CS*) and relative humidity (RH) to calculate the [H_2SO_4], whereas only SO_2 and global radiation are used for the blue triangles.
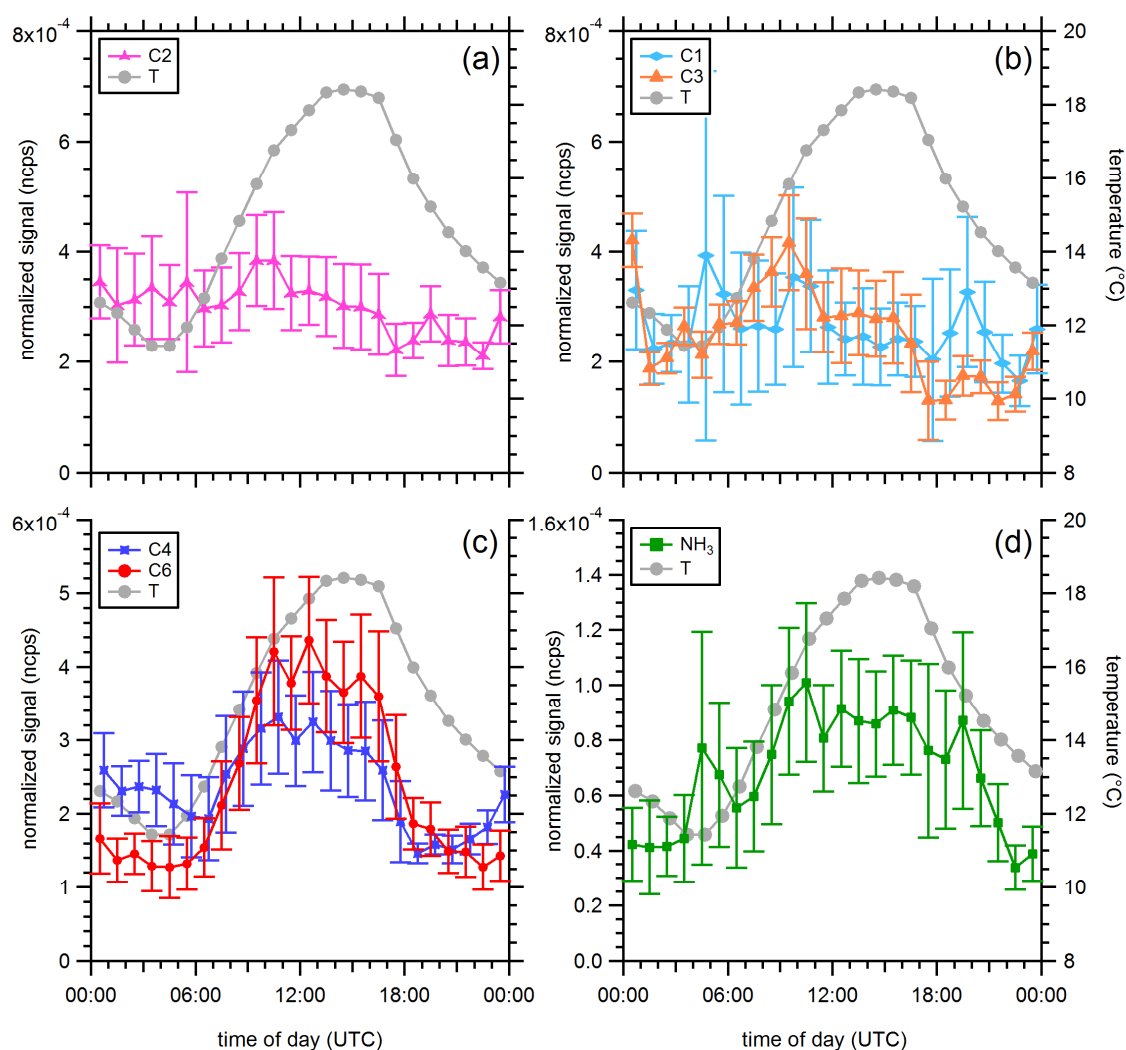
Fig. 5. Diurnal averages for different amines (C1, C2, C3, C4 and C6) and ammonia. The temperature profile is shown in addition. Error bars represent one standard deviation of the 30-minute averages. The lower detection limits for the different compounds are not well-defined, however, the lowest measured signals during some periods were 0.3×10^{-4} ncps for C1, $\sim0.5\times10^{-4}$ ncps for C2, C3, C4 and C6 and 0.1×10^{-4} ncps for ammonia. For most of the time (and for all averaged values shown) the signals were clearly above these "background" levels.
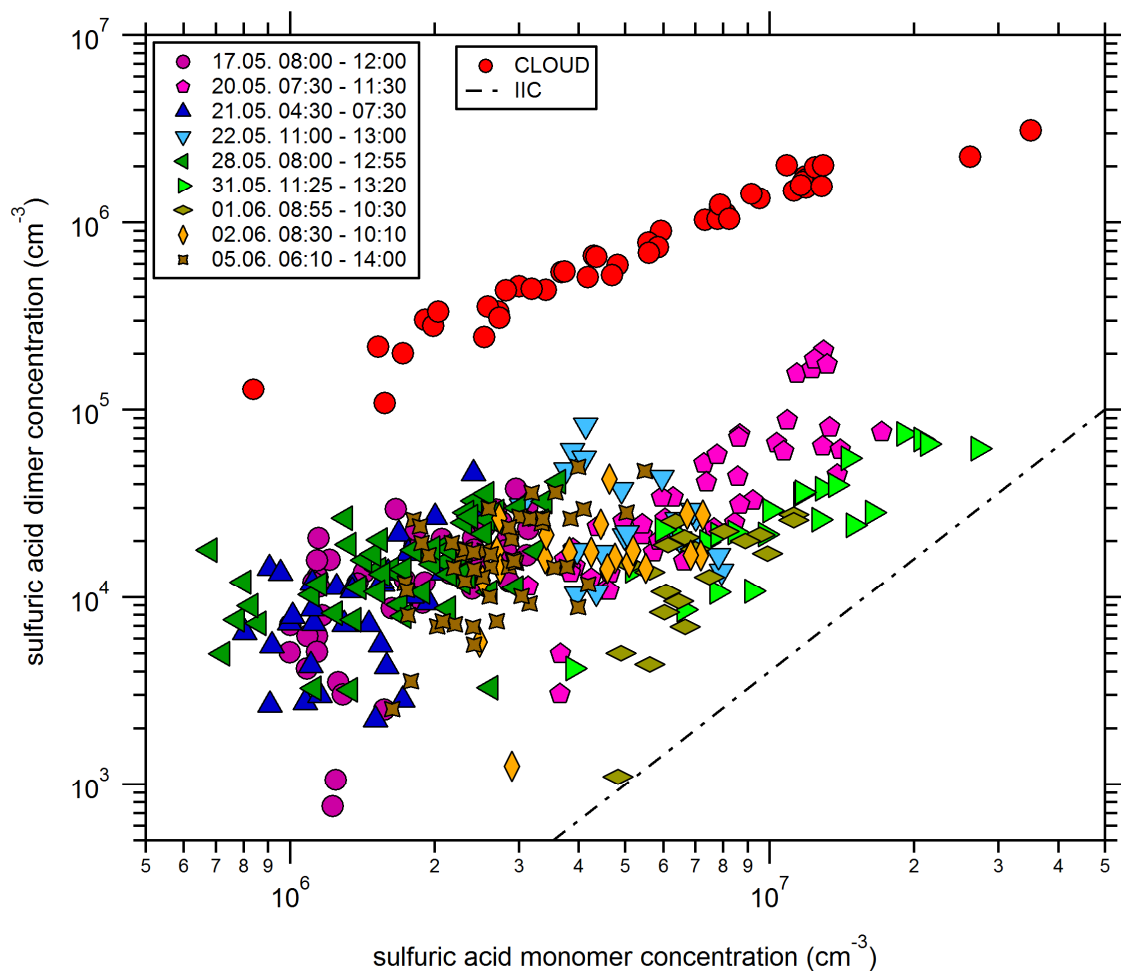
Fig. 6. Sulfuric acid dimer concentrations as a function of the sulfuric acid monomer concentrations. The legend on the left lists the periods when high dimer signals were observed. In addition, data from CLOUD chamber experiments with at least 10 pptv of dimethylamine are shown; under these conditions dimer formation proceeds at or close to the kinetic limit (Kürten et al., 2014). The dashed-dotted line indicates the lower detection limit for neutral dimers set by ion-induced clustering (IIC) within the CI-APi-TOF ion reaction zone.

1314
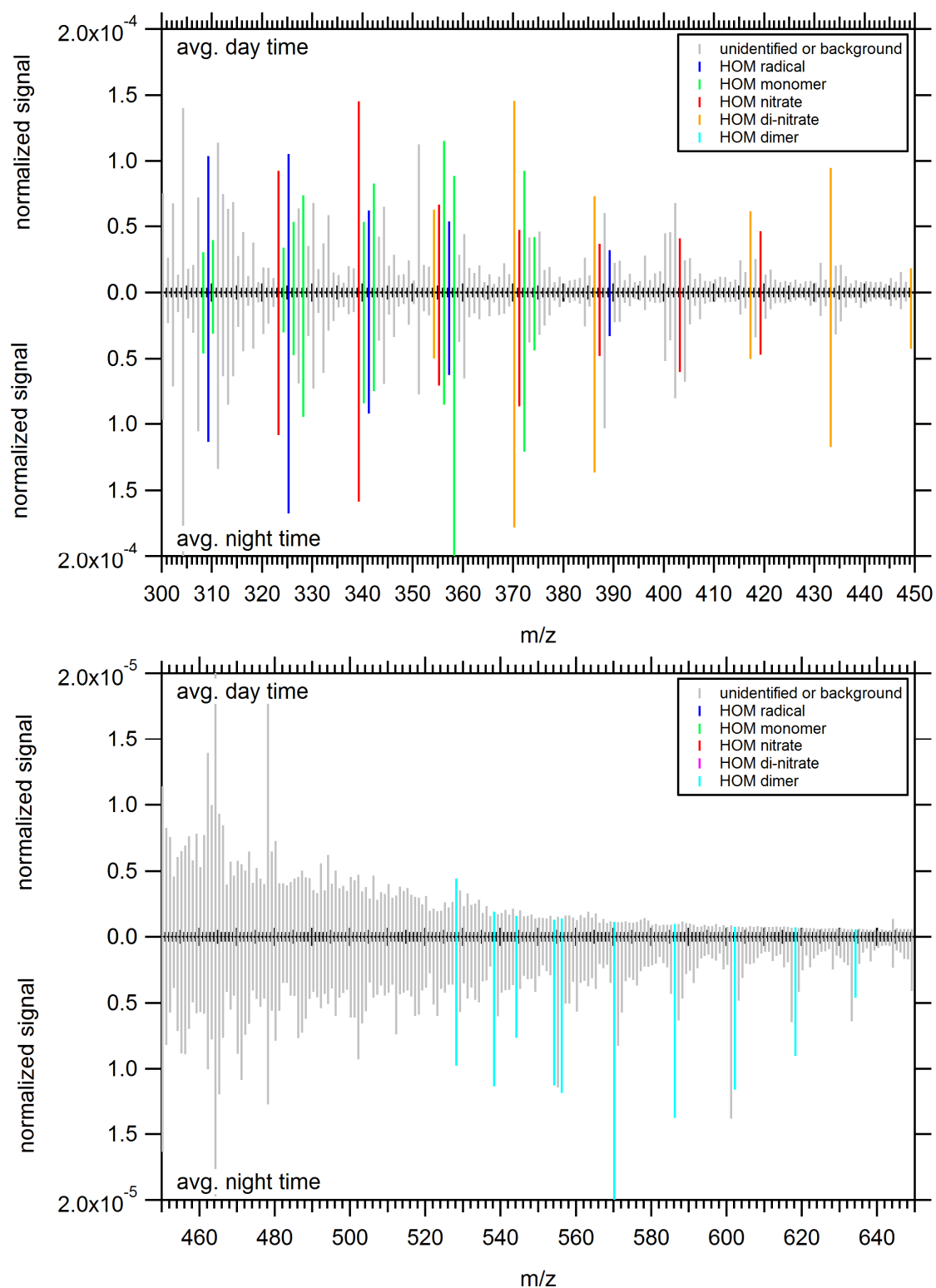
Fig. 7. Comparison between average day time and night time mass spectra measured with the nitrate CI-APi-TOF. The day time spectrum was averaged for periods when no nucleation was observed.

1315

1316
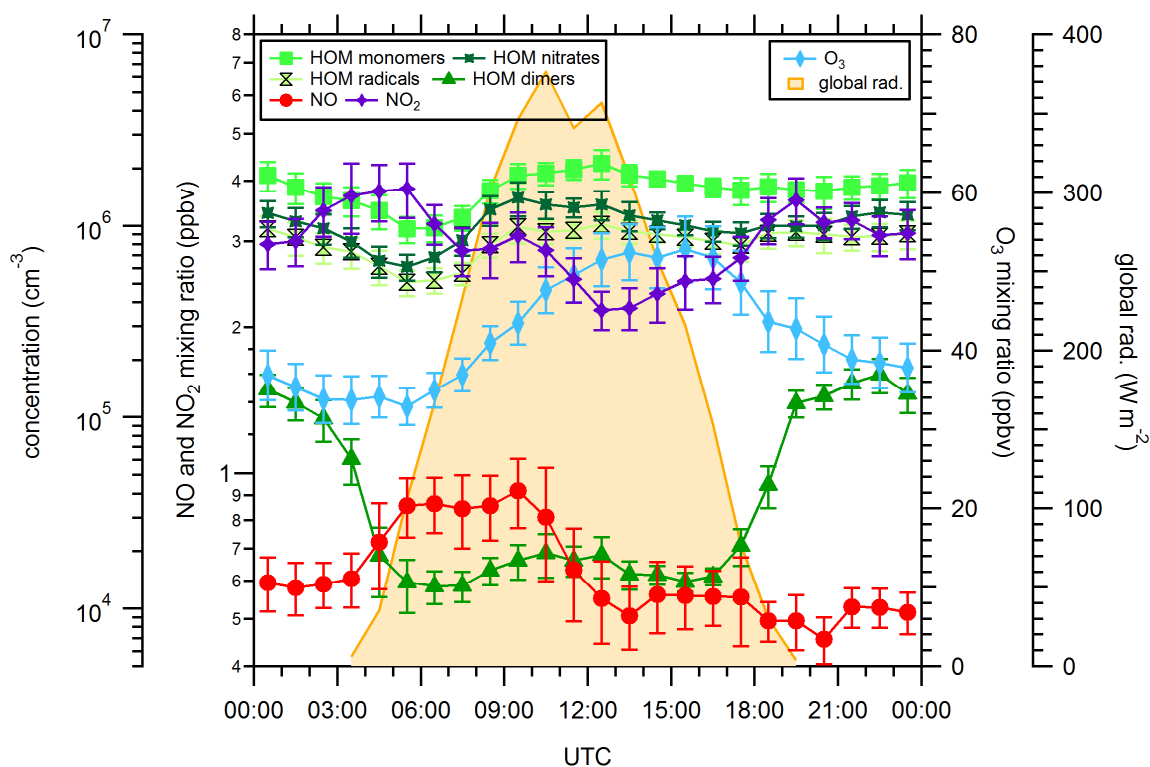
Fig. 8. Diurnal profiles of the NO, NO_2 and O_3 mixing ratios. The signals for highly oxidized organic molecules (HOM) are shown for some C10 (HOM monomers, HOM nitrates and HOM radicals) and C19/C20 compounds (HOM dimers), which show a distinct maximum during the night. The HOM di-nitrates show a similar pattern as the other C10 compounds and are not included in the figure. The global radiation is shown in addition. Error bars indicate one standard deviation for the 30-minute averages.
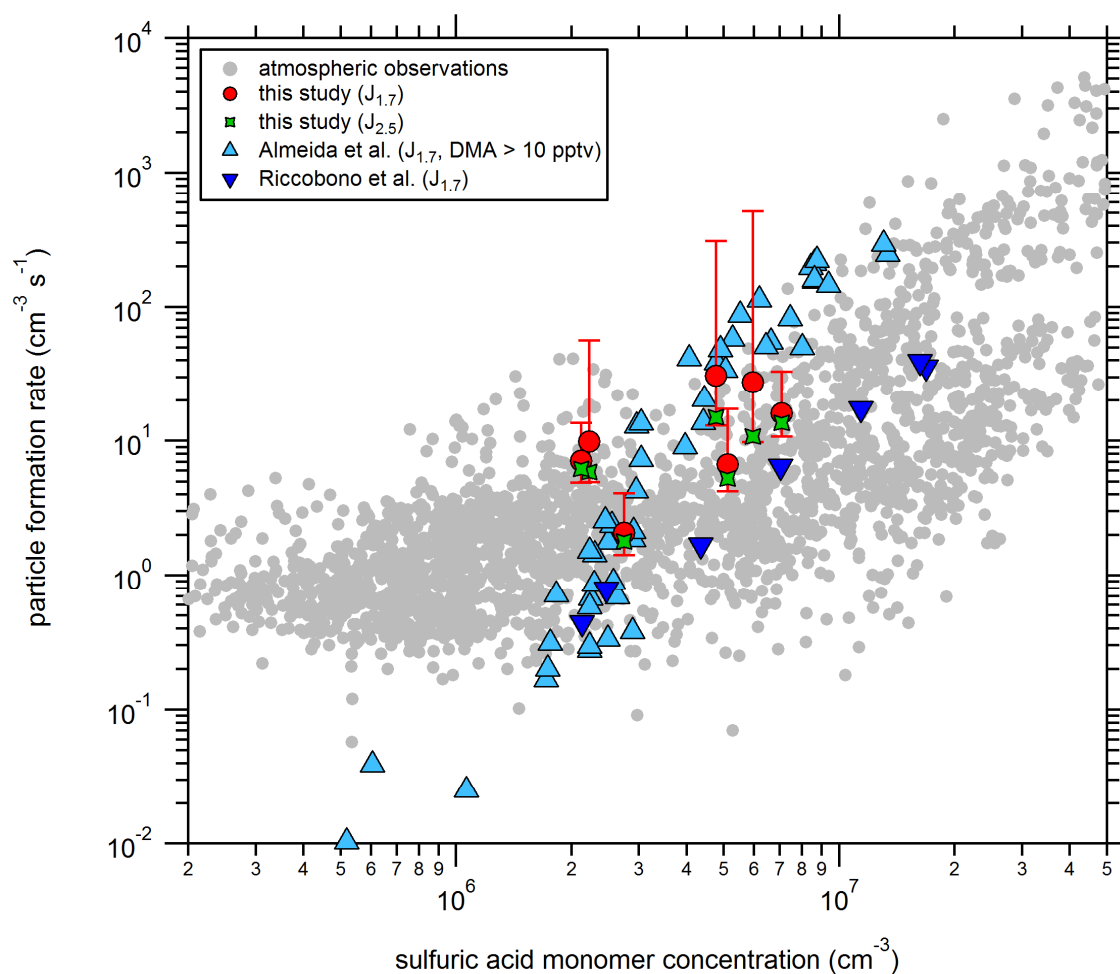
Fig. 9. Particle formation rates from this study at a mobility diameter of 1.7 nm ($J_{1.7}$ red circles) and 2.5 nm ($J_{2.5}$, green stars). Data from CLOUD chamber measurements for a diameter of 1.7 nm are shown in addition for the system of sulfuric acid, water and dimethylamine (light blue symbols, see Almeida et al., 2013) and sulfuric acid, water and oxidized organics from pinanediol (dark blue symbols, see Riccobono et al., 2014). The light grey circles are from other field measurements (Kuang et al., 2008; Paasonen et al., 2010; Kulmala et al., 2013).
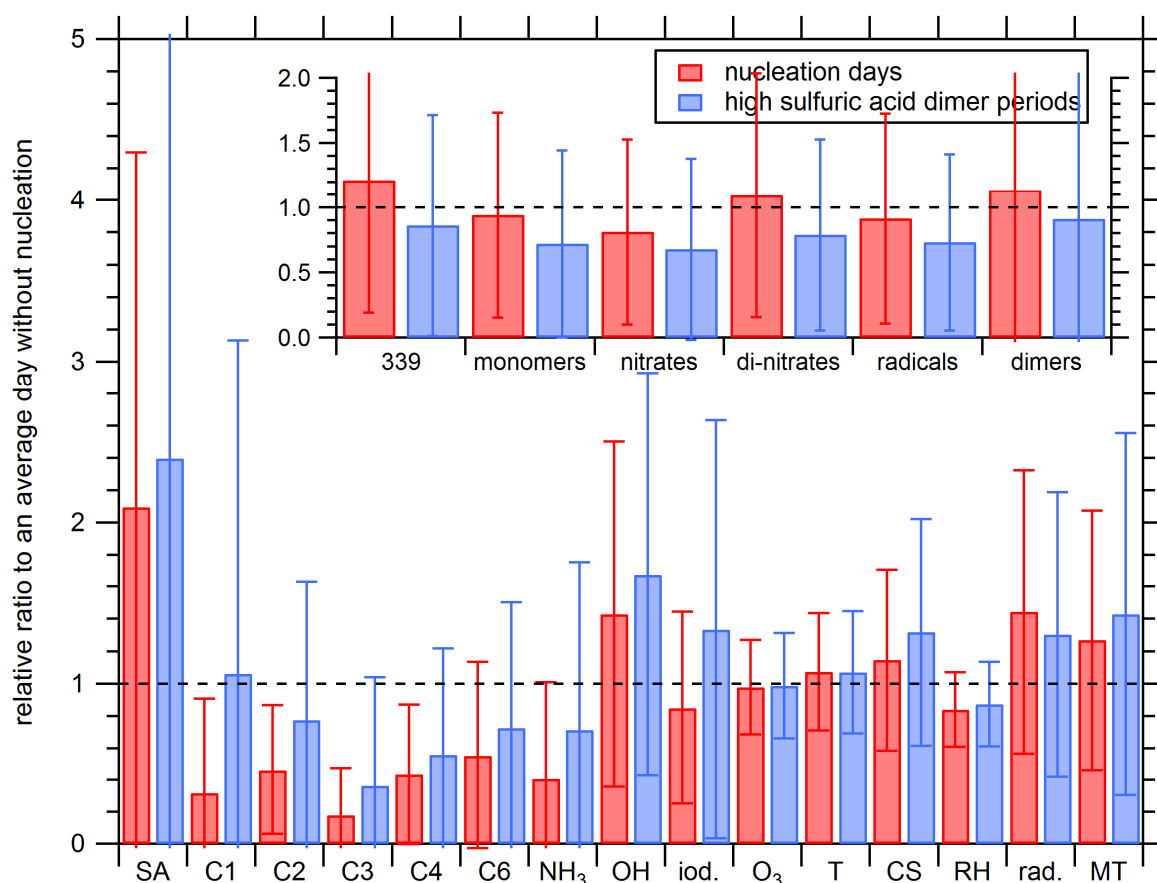
Fig. 10. Comparison of various parameters for different time periods (SA = sulfuric acid monomer, C1, C2, C3, C4 and C6 = amines, iod. = iodic acid and rad. = global radiation intensity). The subset figure on the upper right shows the signals for the highly oxidized organic compounds with 10 or 20 carbon atoms (339 = organic compound $C_{10}H_{15}NO_8$ clustered with NO_3^- having a mass of 339.0681 Th, the definition of other HOM, i.e. monomers, radicals, nitrates, di-nitrates and dimers can be found in Table 2). The red bars relate nucleation days to days without nucleation and the blue bars show the ratio between periods where high sulfuric acid dimer concentrations were observed (see Fig. 6) to no nucleation days. Similar times of the day (early morning) were used as reference periods when no nucleation was observed as nucleation and dimer formation was also mainly observed in the morning.